地震研究所彙報
Bull. Earthq. Res. Inst.
Univ. Tokyo
Vol. 76 (2002) pp. 455-478

Morphology of the Intraslab Seismic Zone and Devolatilization Phase Equilibria of the Subducting Slab Peridotite

Soichi Omori[1]*, Shin'ichiro Kamiya[2], Shigenori Maruyama[1] and Dapeng Zhao[3]

[1] Department of Earth and Planetary Sciences, Tokyo Institute of Technology.
[2] National Research Institute for Earth Science and Disaster Prevention (present address: Institute for Frontier Research on Earth Evolution, Japan Marine Science and Technology Center).
[3] Department of Earth Sciences, Ehime University.

Abstract

The dehydration-induced earthquake hypothesis for intermediate-depth earthquakes in a subduction zone was examined semi-quantitatively in the light of multi-component phase equilibria of the mantle. Based on the expected dehydration equilibria in subducting peridotite, we found a further organized structure in the hypocentral distribution observed in northeast Japan to the double seismic zone (DSZ). The structure of the seismic zone is possibly controlled by a chemical rather than a mechanical process.

We first constructed a phase diagram in the model system MgO-Al_2O_3-SiO_2-H_2O (MASH) using thermodynamic calculations. Then possible hypocenter distributions in subducting mantle were semi-quantitatively predicted on the assumption that: 1) any dehydration induces earthquakes; 2) a subducting slab is more or less hydrated; 3) hydrated mantle is approximated by the MASH model system; and, 4) dehydration proceeds near equilibrium. The predicted topology of dehydration-induced seismic zones reproduces the double seismic zone (DSZ); also predicted are multiple seismic zones, multiple convergences of the seismic planes, and thermal structure dependence of the convergence depth of the DSZ. These predictions are compared to seismic observations in NE Japan and the world's subduction zones. In NE Japan, the geometry of the double seismic zone and the hypocenter clusters between the double seismic planes compare well to the predicted dehydration-induced multiple seismic zones and multiple convergences, assuming a simple prograde P-T path for the coldest thermal center of the slab. The correlation of the age of the subducting plate and the depth of the convergence of the world's DSZ is also consistent with the prediction. The assumption of a hydrated mantle is examined by seismic tomography beneath the Kanto area. The Poisson's ratio calculated between the two seismic planes at a depth ca. 50-80 km suggests the existence of serpentinized peridotite in the subducting mantle at those depths, even though the degree of hydration is not so strong (ca. 50-30%) and is heterogeneous. Transform faults, oceanic fracture zones, and faults at the trench are all considered to be possible hydration sites of the oceanic mantle. Using the dehydration induced-earthquake model, the link between the dehydration and the seismic zone provides us with the thermal structure in the subducting slab. The estimated thermal structure exhibits a higher temperature than previous numerical simulations, particularly within the slab. Our estimate suggests viscous heating has been underestimated in previous numerical simulations and heat transfer by a fluid produced by the dehydration of the slab mantle must be included in the model. The dehydration model is also applicable to deep seismicity in the mantle transition zone.

Key words: dehydration, earthquake, subduction zone, phase equilibria, double seismic zone

*e-mail : omori@geo.titech.ac.jp (2-12-1. Ookayama, Meguro-ku, Tokyo)

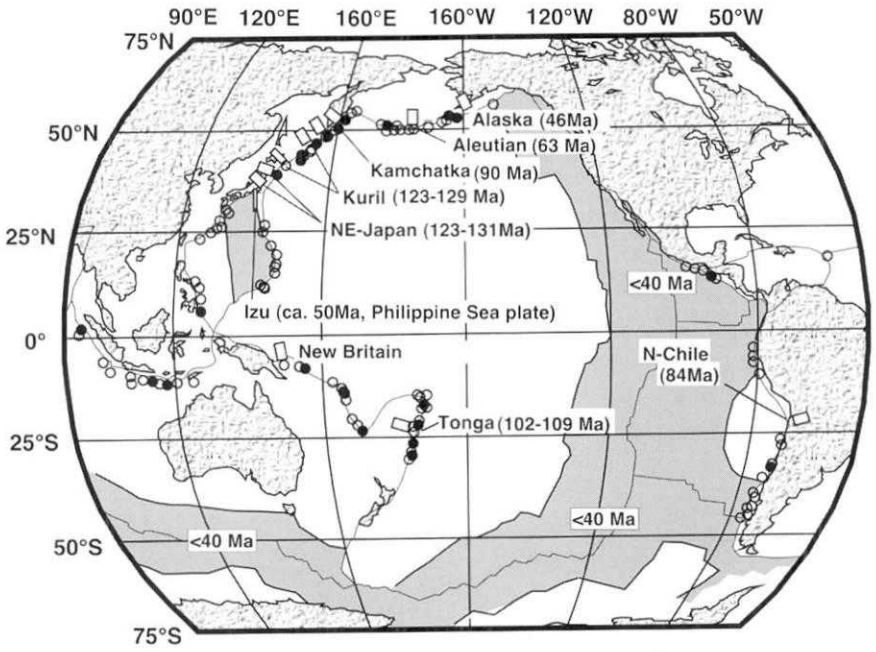

Fig. 1. World map showing the distribution of double seismic zones (modified after Peacock, 2001). Rectangles: double seismic zones, Circles: outer rise earthquakes, Shaded area: oceanic plates younger than 40 Ma.

Introduction

Wadati-Benioff zone is a distinct structure of hypocenter distribution in the subduction zone, and has been known to mark the position of a downgoing oceanic plate, since the paradigm of plate tectonics was established. However, some subduction zones exhibit a double seismic zone (DSZ hereafter) at an intermediate depth of ca. 50–250 km. After the first discovery of a DSZ in NE Japan (Umino and Hasegawa, 1975), DSZs have been reported, rather often, from most subduction zones, except those where a very young lithosphere is subducting, such as Cascadea in N. America and SW Japan. DSZs at an intermediate depth have been confirmed in Alaska-Aleutian Islands (Engdahl and Scholz, 1977; Ratchkovsky *et al.*, 1997), N. Chile (Comte and Suarez, 1994), NE Japan (Umino and Hasegawa, 1975; Zhao *et al.*, 1997), Kamchatka-Kuril (Kao and Chen, 1994; Gorbatov *et al.*, 1994), New Britain (McGuire and Wiens, 1995), Tonga (Kawakatsu, 1985), the Philippine Sea plate subduction zone at Izu (Hori, 1997; Seno *et al.*, 2001) (Fig. 1). However, there remains uncertainty about the hypocenter location and recognition of DSZ should be done carefully; e.g., in the Aleutian subduction zone, some of the hypocentral locations identified by local observations (Engdahl and Schols, 1997) differ from the locations identified by teleseismic observations (Barazangi and Isacks, 1979). Deep earthquakes in the Izu-Bonin subduction zone also exhibit DSZ (Iidaka and Furukawa, 1994). The upper plane of a DSZ at an intermediate depth is separated from the lower plane by about 30–50 kilometers, and the two planes gradually merge as depth increases. In NE Japan (Fig. 2) the upper plane may be partly within the oceanic crust, but the lower plane is definitely within the slab mantle (Zhao *et al.* 1997).

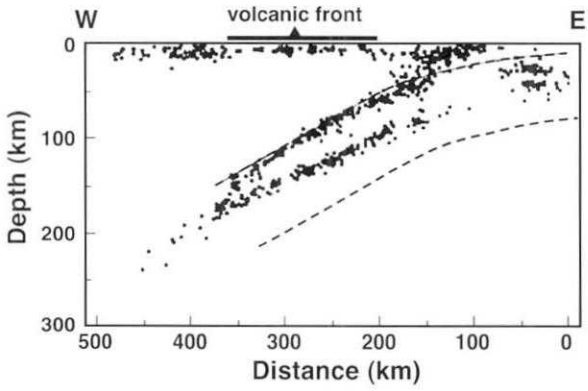

Fig. 2. Vertical cross-section of NE Japan (39 N) showing hypocenter distributions of a typical double seismic zone (Hasegawa *et al.* 1994). Solid curve is estimated upper slab boundary.

The formation of a double seismic zone is one of the major targets to solve the origin of an intraslab earthquake, because it occurs without doubt not along the top shearing surface of the slab, but within the slab. At this depth, peridotite is expected to be ductile at a high-T (Paterson, 1978), hence, some intraslab earthquakes cannot be explained by the brittle-deformation model. Thus an alternative model is proposed to explain a failure at depth. Among intermediate depth earthquakes, upper plane earthquakes were once interpreted to be induced by the dehydration of the hydrated oceanic crust (Kirby, 1995). However, upper plane seismicity seems not to be restricted to a narrow band less than the thickness of the crust, but it expands to as much 30 km, although hypocentral determination errors of as much as 10 km should be included in this estimate. In addition, the oceanic crust contains serpentinite in the form of a solid intrusion. Therefore, reactions in hydrated peridotite should be considered for some part of the upper plane, as well as for lower plane earthquakes. Previously proposed models are metastable garnet formation from Al-enstatite along the isotherm (Kao and Liu, 1995) and serpentine decomposition in the topmost, presumably hydrated, mantle below the capped MORB crust (Nishiyama, 1992; Seno and Yamanaka, 1996; Omori *et al.*, 2000; Peacock, 2001); both are reaction-induced earthquake models in the subducting mantle.

Reaction-induced earthquake models are favored because they seem to be able to explain both the faulting under high-P and T conditions and the morphology of the hypocenter distribution. The relation of dehydration by serpentine decomposition and earthquake was experimentally determined by Raleigh and Paterson (1965) and Meade and Jeanloz (1991) as a dehydration embrittlement of serpentinite. Previous studies (Nishiyama, 1992; Seno and Yamanaka, 1996; Peacock, 2001) emphasized the similarity of the morphology of DSZ and the reaction. Peacock (2001) tried to explain the correlation between serpentine break-down and the lower plane of DSZ using a numerically simulated thermal structure of the subducting slab. However, the result shows a very large discrepancy between the P-T location of the serpentine break-down reaction and earthquake distribution. The range of P-T conditions of lower plane earthquakes is too wide to be explained by single serpentine dehydration (Fig. 3), even though possible uncertainties of hypocentral determination, upon modeling the thermal structure, in the experiments that determined the P-T condition of serpentine decomposition, and some kinetic effects on dehydration are taken into account.

Taking the above problems of Peacock (2001) into consideration, we test how the dehydration-induced earthquake model explains natural earthquakes that occur within subducting mantle with a different approach from the previous study; we do not simulate the thermal structure of a subducting slab, but consider the topological link between dehydration reaction and hypocentral distribution.

In the present study, we start with four assumptions: 1) any dehydration in a subducting slab induces earthquakes; 2) subducting mantle is more or less hydrated; 3) dehydration proceeds in a near-equilibrium condition; and, 4) approximation of hydrated mantle to the MgO-Al_2O_3-SiO_2-H_2O (MASH) system. First, we semi-quantitatively predict the topology of possible hypocenter distributions in a subducting mantle with phase equilibria in the MASH system, which take into account any possible dehydration in the subducting mantle, using a hypothetical thermal structure of a subducting slab instead of numerically modeled one. The topological features of the predicted seismic zone were compared with natural seismic observations in NE Japan. In the light of multi-component dehydration phase equilibria in a hydrated mantle, we found a more organized structure of an intraslab seismic zone than a simple DSZ, with a good correlation between predicted topology and observations. Consequently, we estimated an approximate thermal structure of the slab, on the basis of the above four assumptions, by inversion from the observations of hypocenter distribution. Finally, we emphasize the significance of chemical processes on the genesis and spatial the organization of an intermediate earthquake in the subducting mantle.

Phase relation of hydrated mantle up to 9 GPa

Several high-pressure experimental studies on hydrous phases of mantle composition have produced experimental results which differ; for example, the decomposition temperature of antigorite at 6 GPa ranges from about 300℃ (Wunder and Schreyer,

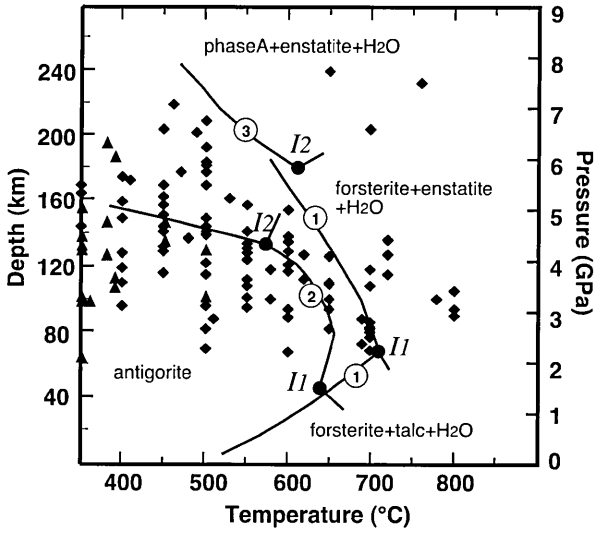

Fig. 3. Comparison of calculated P-T condition of intermediate-depth earthquakes and experimentally determined antigorite decomposition curves (modified after Peacock, 2001). Diamonds: lower plane earthquakes, Triangles: upper plane earthquakes, I_1, I_2: invariant points; I_1 = antigorite + forsterite + enstatite + talc + H_2O; I_2 = antigorite + forsterite + enstatite + phaseA + H_2O, Numbers on the curves: references; 1-Ulmer and Trommsdorff (1995); 2-Wunder and Schreyer (1997); 3-Bose and Navrotsky (1998).

1997) to 600℃ (Bose and Navrotsky, 1998) as shown in Fig. 3. This discrepancy has been considered to be due to kinetic problems and differences in natural starting materials in the experiments. A thermodynamic calculation has an advantage over such low-temperature equilibria, when the data are well constrained by experiments at a high enough temperature to achieve equilibrium. Hence, we constructed a phase diagram of hydrated mantle up to 9 GPa using thermodynamic calculations, although the effects of minor components in antigorite were not taken into account.

The model system MgO-Al_2O_3-SiO_2-H_2O (MASH) was assumed to be applicable to hydrated peridotite. MgO, Al_2O_3, and SiO_2 are the major components in typical lherzolite and they constitute 90 wt% of lherzolite composition; the remaining components are FeO (ca. 6-9 wt%) and CaO (ca. 1-4 wt%). At present, the lack of experimental and thermodynamic data on some Fe end-members of the hydrous phase in the mantle (e.g. antigorite, phase A) prevent inclusion of the FeO component in the calculation. If we take account of CaO in the calculation, clinopyroxene, Ca-amphibole, and the grossular component in garnet can be included in the calculation; however, these components are minor in the peridoritic system. Thus, the MASH model system was chosen for this study, by balancing reliability and simplicity, to discuss the topology of dehydration in the slab.

Table 1 lists phases included in the calculation, their abbreviations, chemical compositions and source of thermodynamic data. Referring to previous experimental studies (e.g. Bose and Navrotsky, 1998; Wunder and Schrayer, 1997, Ulmer and Trommsdorff, 1999), we included 10 hydrous minerals (antigorite, phase A, clinohumite-OH, chondrodite-OH, talc, anthophyllite, brucite, clinochlore, MgMgAl-pumpellyite, and diaspore) and five anhydrous minerals (forsterite, low-P clinoenstatite, high-P clinoenstatite, enstatite , and periclase) in the calculation. Natural serpentinite consists of three serpentine group minerals: antigorite, chrysotile, and lizardite. Chrysotile and lizadite are stable at very low temperatures (<300℃), but antigorite is stable at T> 300℃ (e.g. O'Hanley, 1996), thus we included only antigorite in the calculation. Enstatite was assumed to be a solid solution with tschermak substitution ($MgSiAl_{-1}Al_{-1}$). Figure 4 shows the model bulk composition of the system in the MSH section.

For the calculation we have used an internally consistent thermodynamic dataset of minerals and fluids by Holland and Powell (1998). Enstatite polymorphs, chondrodite, and MgMgAl-pumpellyite, however, are not included in this database, and some calculated reaction curves, e.g., clinochlore decomposition reaction, exhibit different positions from those experimentally determined at a high pressure. Therefore, we have expanded the dataset and corrected some parameters according to recent high-P experimental work. We have estimated the standard state entropies and standard state enthalpies of formation of clinohumite-OH, chondrodite-OH, high-P clinoen statite, low-P clinoenstatite, and MgMgAl-pumpellyite. The thermal expansion and incompressibility of clinochrore, spinel, and pyrope were modified to fit the experimentally determined equilibria. We used the computer program "UniEQ" (Omori & Ogasawara, 1998) for all calculations.

Figure 5 is the constructed petrogenetic grid in the MASH system for a hydrous mantle composition up to 9 GPa, 900℃. The numbers on the curves

Table 1 Phases included in calculation and source of thermodynamic data.

phase	abbreviation	chemical formula	data
Anthophyllite	Ath	$Mg_7Si_8O_{22}(OH)_2$	1
Antigorite	Atg	$Mg_{48}Si_{34}O_{85}(OH)_{31}$	1
Brucite	Br	$Mg(OH)_2$	1
Chondrodite	Chon	$Mg_5Si_2O_9(OH)_2$	2, 3
Clinochlore	Chl	$Mg_5Al_2Si_3O_{10}(OH)_8$	1, 4
Clinohumite	cHum	$Mg_9Si_4O_{16}(OH)_2$	1, 5
Clinoenstatite (high-P)	hcEn	$Mg_2Si_2O_6$	3, 6
Clinoenstatite (low-P)	lcEn	$Mg_2Si_2O_6$	3, 6
Diopside	Di	$CaMgSi_2O_6$	1
Enstatite	En	$Mg_2Si_2O_6$	1
Forsterite	Fo	Mg_2SiO_4	1
MgMgAl-pumpellyite	Mpum	$Mg_5Al_5Si_6O_{21}(OH)_7$	3, 7
Mg-tschermak pyroxene	Mtsch	$MgAl_2SiO_6$	1
Pyrope	Prp	$Mg_3Al_2Si_3O_{12}$	1, 4
Spinel	Sp	$MgAl_2O_4$	1, 4
Talc	Tc	$Mg_3Si_4O_{10}(OH)_2$	1
Enstatite (En/lcEn/hcEn-Mtsch) solid solution	Ens.s.	$(Mg_{1-x},Al_x)_2(Al_x,Si_{1-x})_2O_6$	8
H_2O		H_2O	1
Aragonite	Arag	$CaCO_3$	1
Dolomite	Do	$CaMg(CO_3)_2$	1
Magnesite	Mag	$MgCO_3$	1
CO_2-H_2O fluid	Fld	$(CO_2)_xH_2O_{(1-x)}$	1

1: Holland and Powell (1998); 2: Vs and bulk modulus were taken from Faust and Knittle (1994), $\Delta Hf°_{298}$ and $S°_{298}$ were estimated from Wunder (1998); 3: Cp was approximated by oxide sum; 4: bulk modulus and thermal expansion were modified to fit Ulmer and Trommsdorff (1999); 5: $\Delta Hf°_{298}$ and $S°_{298}$ were estimated from Pawley (2000); 6: $\Delta Hf°_{298}$ and $S°_{298}$, Vs, bulk modulus and thermal expansion were estimated from Shinmei et al. (1999); 7: $\Delta Hf°_{298}$ and $S°_{298}$, Vs, bulk modulus and thermal expansion were estimated from Fockenberg (1998) and Artioli et al. (1999); 8: ideal mixing.

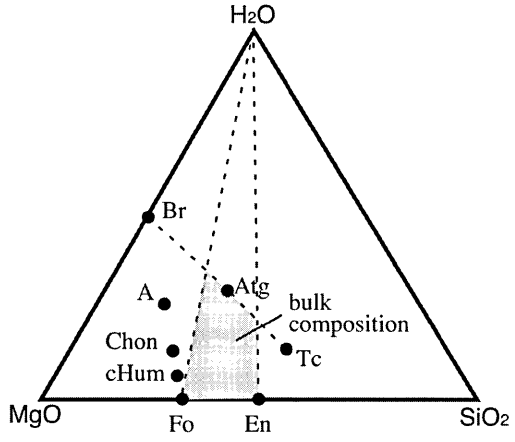

Fig. 4. Composition diagram in MgO-SiO_2-H_2O (MSH) section. Shaded area is model bulk composition for the calculation. For the calculation in the MASH system, clinochlore is assumed to be an initial aluminous hydrous phase, in addition to the MSH hydrated mantle.

correspond to the reactions listed in Table 2. Univariant dehydration curves are represented by solid curves, and solid-solid reactions by dashed lines. Continuous dehydration reactions correspond to clinochlore or MgMgAl-pumpellyite decompositions to form the Mg-tschermak component in enstatite. These reactions occupy an area of the P-T space, which is shaded in the P-T diagram.

Model cross-section of a subduction zone

Using the calculated phase diagram of the hydrated mantle, we can project dehydration curves onto a subduction zone cross-section, if the thermal structure of the subduction zone is defined. Peacock (1996) and Iwamori (1998) undertook numerical modeling of the thermal structure of a subduction zone. Although the model still has considerable uncertainty depending on thermal and mechanical parameters, the common features of the model subduction zone geotherm are: 1) the isotherm in the slab is

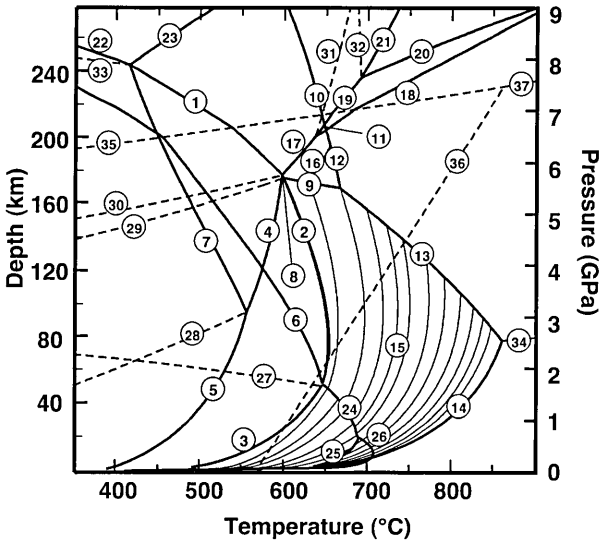

Fig. 5. Calculated P-T diagram in the model system MASH for hydrous mantle up to 9 GPa, 900℃. Abbreviations are shown in Table 1. Numbers on the curves correspond to the reactions in Table 2. Thick solid lines: univariant dehydration reactions, thin solid lines: continuous dehydration reactions, dashed lines: solid-solid reactions.

Table 2 Reactions in Fig. 5.

No.	reactions
1	5 Atg = 14 phA + 71 lcEn/hcEn + 113 H_2O
2	Atg = 14 Fo + 10 lcEn + 31 H_2O
3	Atg = 18 Fo + 4 Tc + 27 H_2O
4	20 phA + 3 Atg = 142 Fo + 153 H_2O
5	Atg + 20 Br = 34 Fo + 51 H_2O
6	Atg +Tc = lcEn + H_2O
7	Atg + 71 Br = 17 phA + 51 H_2O
8	Atg + Chl = Fo + Mpum + H_2O
9	Ens.s. + Chl = Fo + Mpum + H_2O
10	phA + Ens.s. + Mpum = Prp + H_2O
11	cHum + Ens.s. + Mpum = Prp + H_2O
12	Fo + Ens.s. + Mpum = Prp + H_2O
13	Ens.s. + Chl = Fo + Prp + H_2O
14	Chl = Fo + Ens.s. + Sp + H_2O
15	lcEn/En in Ens.s. + Chl = Mgts in Ens.s. + Fo + H_2O
16	lcEn in Ens.s. + Mpum = Mgts in Ens.s + Fo + H_2O
17	2 phA + 3 lcEn = 10 Fo + 6 H_2O
18	lcEn/hcEn + 2 cHum= 10 Fo + 2 H_2O
19	lcEn/hcEn + phA = cHum + 2 H_2O
20	hcEn + 5 Chon = 3 cHum + 2 H_2O
21	2 hcEn + 3 phA = 5 Chon + 4 H_2O
22	Atg = 17 hcEn + 14 Br + 17 H_2O
23	hcEn + 5 Br = phA + H_2O
24	Fo + Tc = En + H_2O
25	4 Fo + 9 Tc = 5 Ath + 4 H_2O
26	2 Fo + 2 Ath = 9 En + 2 H_2O
27	90 Fo + 62 Tc = 135 En + Atg
28	phA = 2 Fo + 3 Br
29	Ens.s. + Chl = Fo + Atg + Mpum
30	62 phA + 153 lcEn = 152 Fo + 6 Atg
31	10 Fo + phA = 3 cHum
32	2 cHum + phA = 5 Chon
33	17 phA + 2 Atg = 51 hcEn + 113 Br
34	Ens.s. + Sp = Fo + Prp
35	hcEn = lcEn
36	lcEn = En
37	hcEn = En

strongly convex toward depth along the subducting slab; 2) the coldest thermal center is below the slab upper-boundary, if the subducting plate is not young ; and, 3) the P-T relation of this cold thermal center shows a relatively high positive P/T ratio. According to these basic features, we semi-quantitatively modeled the possible thermal structure in the subducting slab. Fig. 6 shows three model P-T paths for the coldest thermal center in the slab and selected possible dehydration reactions during subduction. It should be noted that the P-T condition of any part of the slab mantle exists at the higher-T side than this model P-T path, because this path represents the coldest temperature at any depth. Figure 7 is the model slab cross-section with projected dehydration reactions derived from the P-T paths in Fig. 6. In Fig. 7, each thick solid line with an arrow corresponds to the model P-T paths in Fig. 6. The thick dashed line is the approximate boundary of the slab, and thin dashed lines are apparent isotherms along the model P-T path of the coldest thermal center. Because the thermal structure presented here was not produced from strict modeling, no horizontal scale is given on the sections, and the top-sitting oceanic crust of the subducting plate is not included in these diagrams. Thick solid lines and circles represent the dehydration reaction curves and invariant points in Fig. 6, respectively. Shaded areas comprise continuous dehydration.

The dehydration reactions depicted in Fig. 7 are considered to be relevant to earthquakes because of the following assumptions: 1) not only antigolite break-down, but also the other dehydration reactions induce embrittlement and earthquakes in a subducting slab, and 2) dehydration proceeds at near-equilibrium. Earthquakes may occur on the univariant reaction curves, and in an area of continuous reactions. Hereafter we regard the dehydration reactions in Fig. 7 as seismic hypocenters. The model cross-sections of the subducting slab in Fig. 7 show the distinctive structure of a dehydration-induced

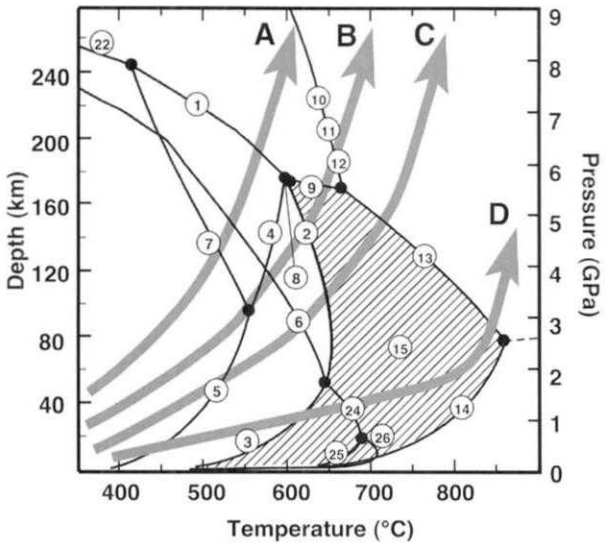

Fig. 6. Model P-T paths for the coldest thermal center of a subducting slab, and selected dehydration reactions that are possible in the subducting slab.

seismic zone up to 250 km in depth. Each section shows so-called double seismic zones, their multiple convergence, and also that they are made by a combination of multiple seismic zones. The number of convergences reflects the total number of intersections of the model P-T path of a cold thermal center and the dehydration curves, and the depth of each convergence corresponds to the pressure of each intersection. The colder P-T path A predicts four pairs of seismic zones and convergences. Most outer seismic zones consist of a continuous seismic area and the deep end of the seismic zone is composed of dehydration of MgMgAl-pumpellyite, instead of antigorite dehydration. Five pairs of seismic zones and convergences are predicted for the model P-T path B. Most outer seismic zones and their convergence are formed by a continuous zone. The P-T path C shows there are three pairs of seismic zones and convergences. Most outer seismic zones and their convergence are also formed by continuous dehydration. Path D is the highest temperature model, and shows intraslab earthquakes distributed as a single seismic zone, instead of DSZ.

The predicted dehydration topologies suggest two significant features of a dehydration-induced seismic zone: 1) multiple convergence of the seismic zones and 2) correlation between the geotherm and the depth of convergences indicates that the high-T P-T path of the coldest thermal center moves the

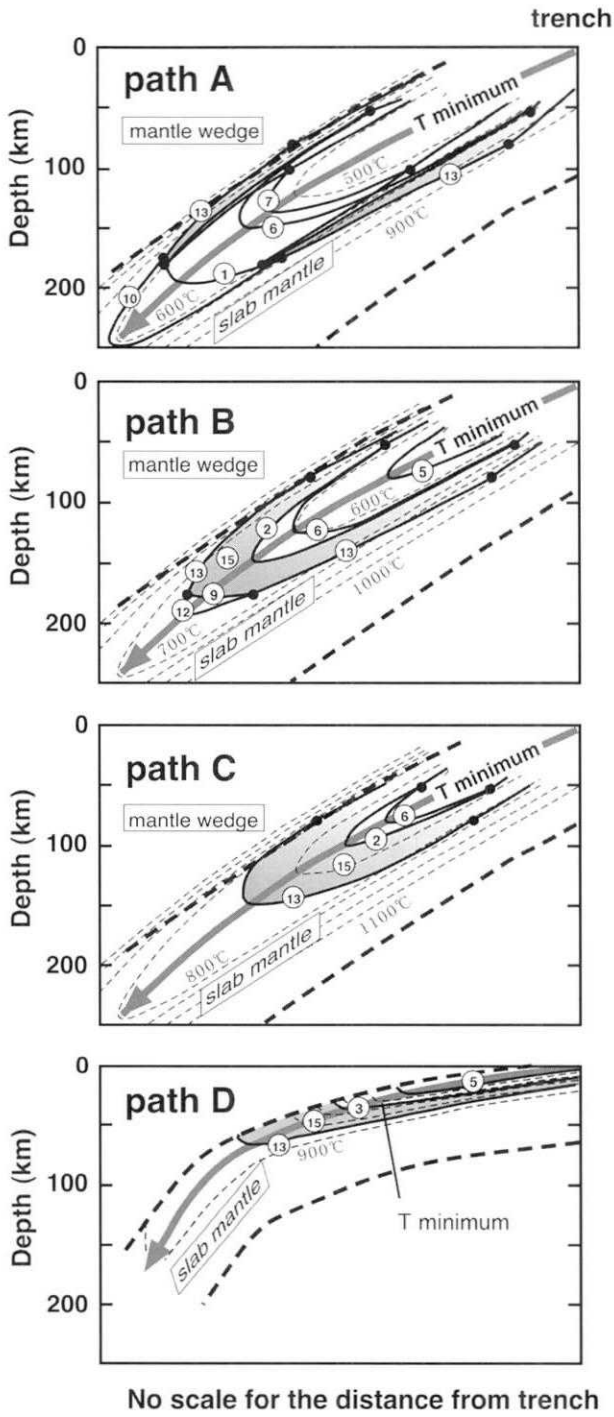

Fig. 7. Model cross-sections of subduction zone and predicted topologies of dehydration reactions that are considered to be dehydration-induced seismic zones. Each section corresponds to the model P-T path for the coldest thermal center in Fig. 6. Solid line: dehydration reaction with numbers of dehydration reaction in Table 2; Shaded zone: continuous dehydration zone; Gray solid line with arrow: coldest thermal center of the slab; Thick dashed line: hypothetical slab boundary; Thin dashed line: apparent isotherm in the model slab.

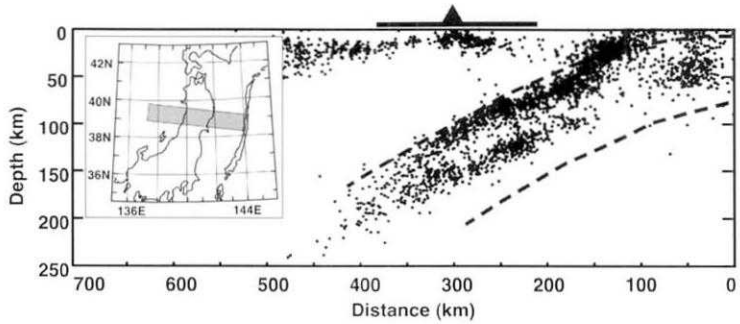

Fig. 8. Vertical cross-sections of NE Japan at 100 km width along the profiles. Dots are locations of earthquakes from Japan University Network Earthquake Catalog from 1985 to 1993. Dashed lines are approximate boundaries of the slab. Upper boundary after Zhao *et al.* (1997).

convergence to a shallower depth. In path D, where the youngest slab subducts, earthquakes occur only at depths shallower than 80 km. In the next section, we compare these features of a predicted dehydration-induced seismic zone with natural hypocenter distributions. First, we examine the multiple convergence using high-precision hypocenter data for the subducting Pacific plate in NE Japan. Then, by compiling the world's DSZ, we analyze the correlation between a P-T path and morphology of intraslab seismic zones.

Dehydration-induced structure of intermediate-depth intraslab earthquakes in NE Japan

NE Japan in the western Pacific, where a 120–130 Ma old Pacific plate is subducting, is one of the best studied subduction zones. To see the structure of the intraslab seismic zone, we projected hypocenters up to 250 km depth onto a vertical cross-section of the subduction zone using hypocentral data from the Japan University Network Earthquake Catalog from 1985 to 1993. Fig. 8 is a 100 km thick cross-section along the profile. An approximate upper boundary of the subducting slab is shown with a dashed line following to Zhao *et al.* (1997). The cross-section exhibits typical features of a DSZ: two planes are separated by ca. 40 km thick, almost blank zone with less seismicity; two planes seems to merge at a depth of around 150–200 km; the lower plane occurs at the center of the subducting slab; and, both upper and lower planes have a thickness of ca. 30 km.

In addition to the DSZ, there are hypocenter clusters between the two seismic planes below 40–50 km from the upper boundary of the slab. We define these earthquakes as interplane earthquakes. Hypocenters also exist at more than 200 km in depth of the post-convergence of the double planes.

We compare these features with the predicted topology of a seismic zone in the previous section. The possible topology of a dehydration-induced seismic zone depends on the thermal structure of the slab. In the present study, we do not use a numerically simulated thermal structure of the slab. To make the link between the observed hypocenter distribution and prediction without a thermal structure, it is necessary to compare prediction and observation with the whole morphology of a hypocenter distribution. If the observed morphology of the seismic zone is totally linked to the predicted structure and if the P-T path, which is necessary to establish the link, is reasonable, it will be confirmed that the intraslab seismic zone has a close correlation with dehydration reactions in the subducting mantle.

Although the distinct multi-zonal structure of the hypocenter distribution predicted in Fig. 7 is not clearly observed in the cross-section in Fig. 8, the existence of interplane earthquakes is obvious. If those hypocenters are clustered at specific depths, they possibly represent a part of the multiple convergence shown in Fig. 7. We statistically analyzed hypocenters at every 5 km in depth within a 15 km width band at the approximate center between the two planes (Fig. 9 a). Fig. 9 b shows depth-frequency relations of interplane earthquakes at depths greater than 80 km. Fig. 9 c shows histograms averaged at every 15 km depth-range to see the distribution of interplane earthquakes. The depth distribution of interplane earthquake in the section has some peaks. Identified peaks in Fig. 9 c exist at the depth in approximate full width at the half-maximum depth

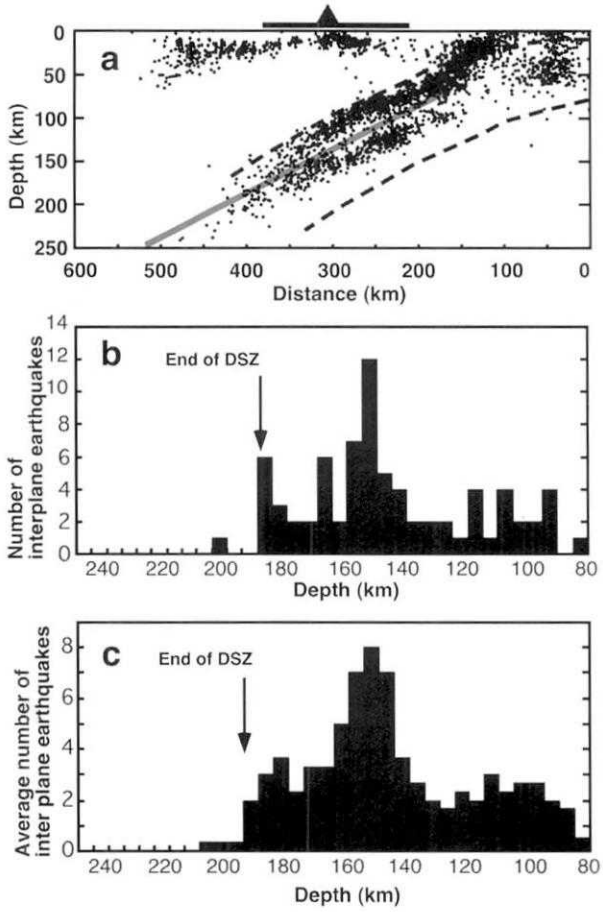

Fig. 9. a) Cross-section of NE Japan. Shaded zone between the two planes is profiled by counting the number of earthquakes in Fig. 9b. b) Depth-frequency relation of the interplane earthquakes along the profile in Fig. 9a. Each column represents the number of earthquakes in a 5 km range of depths. c) Depth-frequency relation averaged in each 15 km.

range of 85–130 km (100 km at max.), 145–170 km (150 km at max.), and 170–195 km (180 km at max.). Although the number of hypocenters comprising the interplane seismic cluster is less than that in double planes, the depth-frequency relationship shown in Figs. 9b and 9c suggests the existence of an organized structure of interplane earthquakes; hence such interplane earthquakes may be compared to the predicted convergences inside the double planes.

Figure 10 shows the correlation between the depth of interplane earthquakes and possible dehydration at that depth. At each depth-range of interplane earthquake, there are several possible dehydration reactions depending on temperature. For the peak at 85–130 km five discontinuous reactions (2, 5, 6,

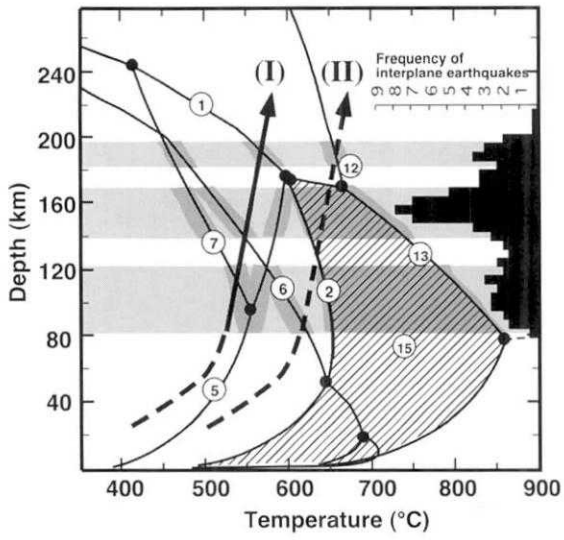

Fig. 10. P-T diagram with superimposed depth-frequency relations of interplane earthquakes in the cross-section in Fig. 8. Light shaded areas represent possible pressure conditions of the interplane earthquakes. Dark shaded areas are P-T conditions where a reaction curve intersects the pressure of interplane earthquakes. Arrows are possible P-T paths for the coldest thermal center of the slab.

7, and 13) and continuous reaction 15 explain the interplane earthquakes well. Similarly, reactions 2, 6, 7, 13, and 15 are the best candidates for the peak at 145–170 km and reactions 6, 7, 1, and 12 for 170–195 km. According to the model thermal structure of a subduction zone provided by any numerical modeling, it is likely that part of the subducting slab mantle >50 km depth follows a simple P-T path with a positive slope during subduction (e.g. Peacock, 1996 ; Iwamori, 1998). Therefore, we can identify which dehydration reaction corresponds to the interplane earthquakes, by choosing the temperatures of dehydration located on a single P-T path with a positive slope. As a result, two possible P-T paths for the coldest thermal center in the slab can be considered (Fig. 10). The colder path (I) in Fig. 10 corresponds to the model P-T path A in Fig. 6, and the corresponding topology of the seismic zone is described by Fig. 7, and the hotter path (II), corresponding to the model P-T path B in Fig. 6 and the model cross-section of Fig. 7.

Although it is difficult to determine which P-T path, (I) or (II), is closer to the real thermal structure of NE Japan only from the distribution of interplane

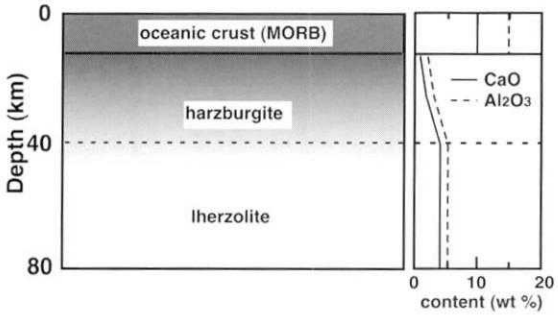

Fig. 11. Model cross-section of the oceanic plate in the NE Japan subduction zone showing chemical differences in the layers.

earthquakes, we can consider that path (I) is better than path (II) to explain the hypocenter distribution of dehydration-induced earthquakes for the following reasons. If the coldest thermal center of the slab followed path (II), the earthquakes near the end-convergence of DSZ correspond to the decomposition of MgMgAl-pumpellyite or clinochlore. However, the existence of MgMgAl-pumpellyite and clinochlore is constrained by the Al-content in the mantle, and a relative high content of Al is limited to lherzolitic mantle, rather than harzburgite, which is considered to exist in a zone several tens of kilometers below the Moho. In NE Japan, a 130 Ma oceanic plate should have a 50 km thick harzburgite layer (Fig. 11) ; accordingly, earthquakes in the upper plane and at the point of convergence must be within the harzburgite layer. The aluminum content in harzburgite (< 1 wt%) is lower than that of lherzolite (4–5 wt%), thus Al-bearing minerals are not expected to be present in the harzburgite layer, and dehydration of clinochlore or MgMgAl-pumpellyite should not occur in the harzburgite layer. These compositional constraints on Al-bearing phases are inconsistent with the observed hypocenter distribution in NE Japan, therefore, P-T path (II) must be rejected. On the other hand, in the case of path (I) earthquakes near the end-convergence correspond to the depth limit of the dehydration of antigorite, so the compositional constraints may be clear if the mantle were hydrated. According to the model cross-section for colder path A in Fig. 7, observed hypocenters deeper than 200 km are interpreted to represent the dehydration of MgMgAl-pumpellyite. These post-convergence earthquakes seem to be an extension of the lower plane (Fig. 9) and occur in the lherzolite layer. Therefore, path (I) is more consistent with the natural observations than hotter path (II). The consistent relationships between the prediction and the observation suggest that: 1) interplane earthquakes may correspond to specific type of dehydration; and, 2) the P-T path for the coldest thermal center, which reliably correlates the dehydration and hypocenter distributions, most strongly supports the dehydration-induced earthquake hypothesis.

Regional heterogeneity of hypocenter distribution in NE Japan

We examine here other profiles of the subduction zone in NE Japan to see regional differences in the morphology of the DSZ. Figure 12 illustrates seven cross-sections, each 50 km wide in NE Japan, and Fig. 13 shows the correlations between depth of interplane earthquakes and dehydration, together with the probable P-T path for the coldest center in the slab of each profile. The DSZ can be seen in all sections, although the lower plane is weak in some sections. The cluster of interplane earthquakes exhibits regional heterogeneity, but the correlations between the depth of the clusters and the dehydration reactions are similar to the section in Fig. 10, and possible P-T paths for the coldest thermal center of the slab are located in a temperature range of 75℃.

Case studies in the world's subduction zones

We now examine other subduction zones to test the applicable range of the dehydration-induced earthquake model. Figure 14 shows representative cross-sections of eight subduction zones around the world taken from previous studies. Because of the fewer number of observations and accuracy in these subduction zones than for NE Japan, we only qualitatively compare the morphology of the seismic zone with the prediction. We choose plate-age at the trench (At) as the principal parameter of the subduction zone to discuss the correlation between the thermal structure and the morphology of a seismic zone. The values of At were taken from Gorbatov and Kostoglodov (1997).

The Kuril subduction zone has a similar At to the NE Japan (ca. 130 Ma) and similar morphology. The fact that the upper and lower planes merge at about 180 km and some interplane earthquakes cluster at ca. 80 km, 100 km, and 150 km is consistent with the

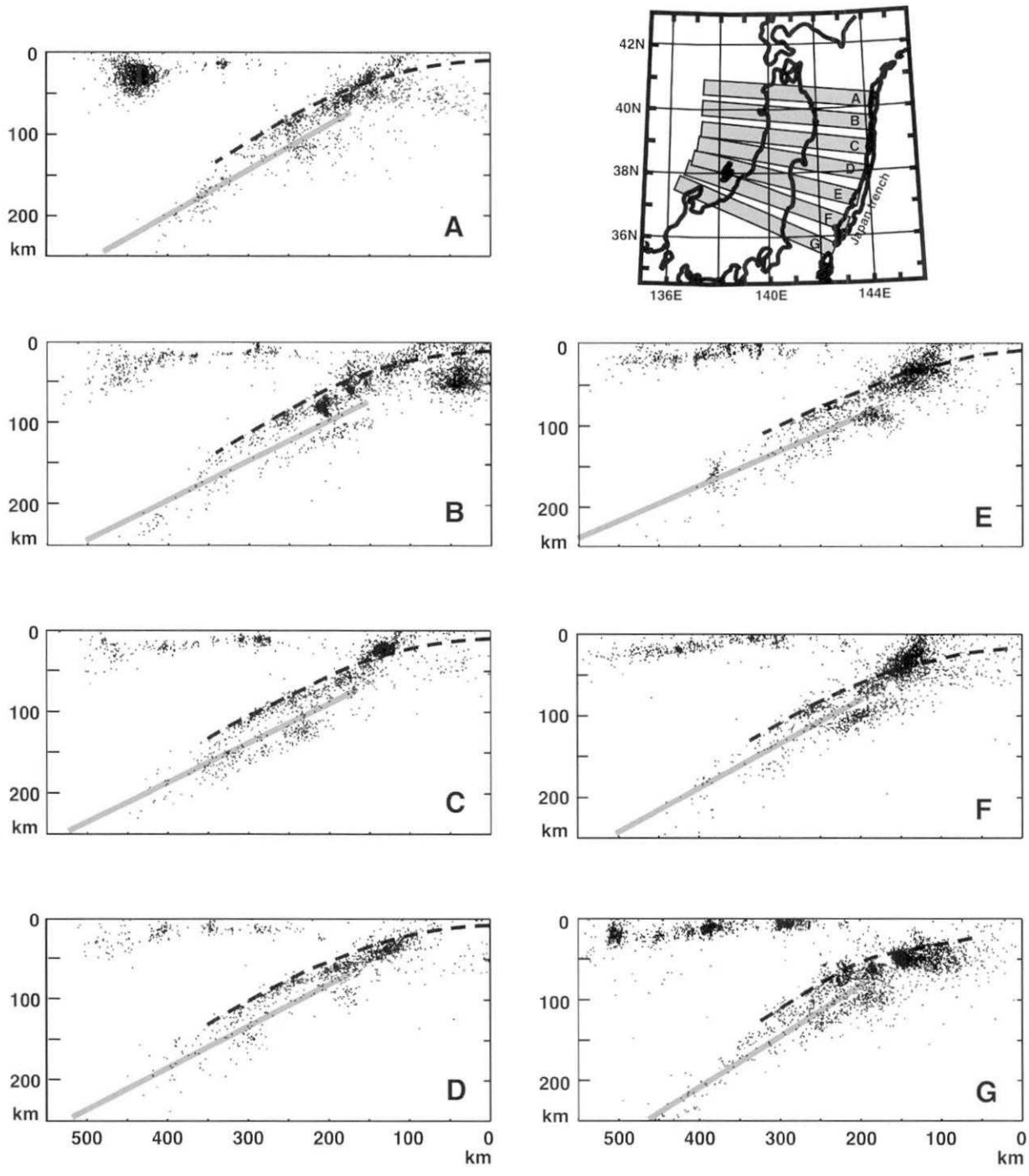

Fig. 12. Cross-sections of NE Japan; each is 50 km wide. Shaded zone between the two planes is profiled by counting the number of earthquakes in Fig. 13.

prediction of cold subduction, model A or B in Fig. 7. Tonga is a subduction zone with At of 109 Ma. A possible DSZ is recognized by Kawakatsu (1995) from an analysis of the focal mechanism, although the geometric separation of the seismic zones is not clear. In this section, earthquakes occur deeper than 250 km, and this observation suggests a similarity with the prediction of model A in Fig. 7, although an apparent cluster of interplane earthquakes is not recognized. Kamchatka is a subduction zone with At of 92 Ma. Possible interplane earthquakes exist below a depth of 50 km. Separation of the two planes

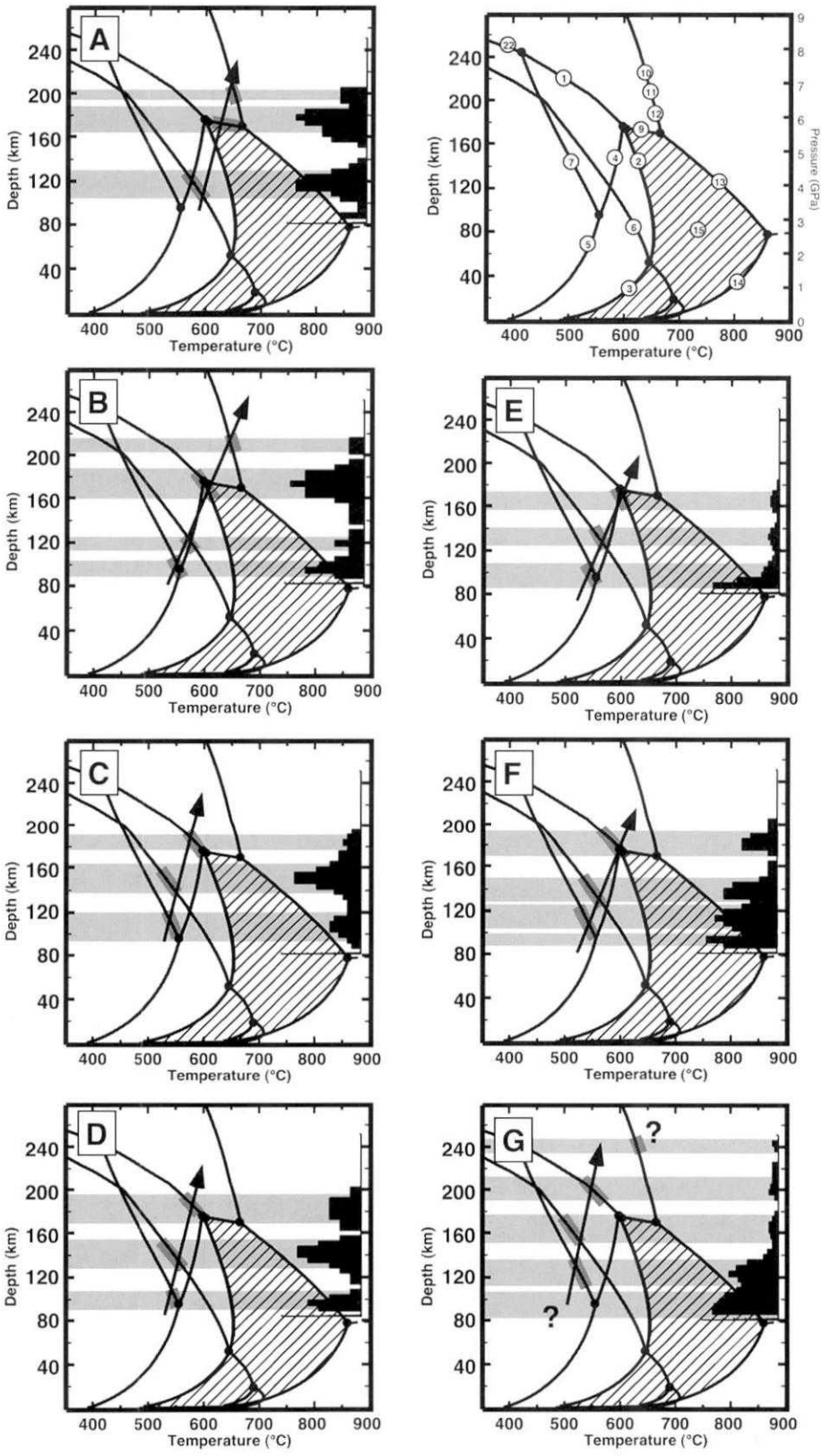

Fig. 13. P-T diagrams with superimposed depth-frequency relation of interplane earthquakes in the cross-sections in Fig. 12. Light shaded areas represent possible pressure conditions of interplane earthquakes. Dark shaded areas are P-T conditions where reaction curves intersect the pressure of interplane earthquakes. Arrows are possible P-T paths for the coldest thermal center of the slab.

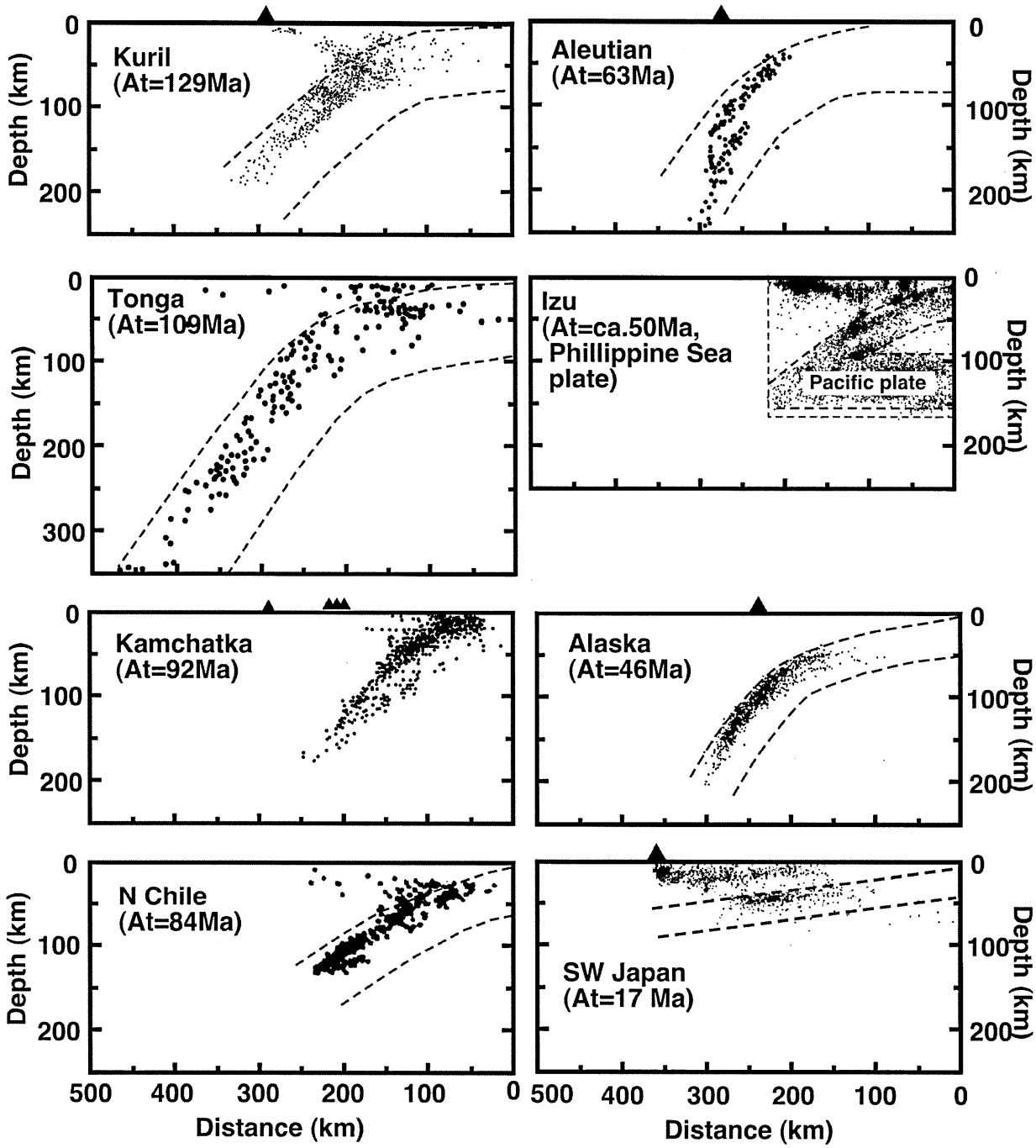

Fig. 14. Vertical cross-section of the world's subduction zones. Source of data: Kuril=Ozel and Moriya (1999), Tonga=Kawakatsu (1995), Kamchatka=Gorbatov *et al.* (1994), N Chile=Comte and Suarez (1994), Aleutian=Engdahl and Scholz (1977), Izu=Kamiya and Kobayashi (2000), Alaska=Ratchkovsky *et al.*, (1997), SW Japan=this study. At: Age of plate at the trench.

becomes indistinct from a depth of ca. 100 km, and the end of DSZ is at a depth of ca. 180 km. This feature corresponds to model B or C in Fig. 7. Northern Chile is a subduction zone of At=84 Ma. Two seismic planes merge at ca. 130 km and DSZ ends at this depth, but the lower plane at a shallower depth is not obvious. The distance between two planes is closer than in NE Japan. Some hypocenters are located between the two planes at a depth of ca. 80 km. This feature corresponds to model B or C in Fig. 7. The Aleutian subduction zone with At=63 Ma exhibits a convergence of the upper and lower planes

at 180 km, and below this depth, the lower plane extends to deeper than 200 km. This feature is interpreted by model A in Fig. 7. The Izu subductioin zone, where Philippine Sea plate ($At \approx 50$ Ma) is subducting northward, exhibits DSZ with the lower plane near the lower boundary of the slab. The convergence depth is not clear because of overlapping seismicty with the Pacific plate. At the subduction zone of Alaska, the Pacific plate ($At = 46$ Ma) is subducting. The hypocenter distribution exhibits a DSZ, which merges at ca. 80 km and thereafter a broad single zone continues down to a depth of 200 km. The existence of this broad single zone following the DSZ corresponds to the hotter subduction of model C in Fig. 7. Southwest Japan is an example of young subduction ($At = 17$–30 Ma) without a double seismic zone. Most of the earthquakes are located in the oceanic crust, but some are in the slab mantle. The distribution of hypocenters demonstrates a single zone, which is ca. 30 km thick. The maximum depth of the earthquakes is ca. 70 km. Such a distribution of hypocenters corresponds to the high-T subduction zone model D in Fig. 7.

In the comparisons above, the variations of hypocenter distributions in the world's subduction zones is correlated to differences in the thermal structure of the slab. The subduction zones of $At >$ 100 Ma including NE Japan, Kuril, and Tonga are considered to have a colder thermal structure; Kamchatka ($At = 96$ Ma) and northern Chile ($At = 84$ Ma) are of the intermediate type; Alaska ($At = 46$ Ma) is relative high-T; and the youngest SW Japan ($At = 17$ –30 Ma) is of the high -T type. These observations are consistent with the first order approximation that the subducting slab with older-At is colder, while the slab with younger-At has a hotter geotherm at a constant dip of the subduction, although shear stress and subduction speed are also important factors for the thermal structure of subduction zone (Peacock, 1996). The Aleutian subduction zone has a younger-At (63 Ma) and was interpreted to have a colder thermal structure, because of the existence of earthquakes deeper than 200 km. This case does not follow the simple At-temperature relation. This exception is considered to be due to a steeper dip of than other subduction zones. Similarly, in the Alaska subduction zone, the subduction dip becomes steeper with depth. This may be the reason why the end of seismic zone reaches ca. 200 km instead of its younger-At.

Our observations and interpretations of the representative subduction zones show that the dehydration-induced earthquake model is possibly applicable to these subduction zones. The variation of the morphology of intraslab seismic zones is considered to represent differences of thermal structure in each subdaction zone.

Discussion

Starting from four basic assumptions: 1) earthquakes are induced by dehydration; 2) the mantle is hydrated; 3) dehydration is in equilibrium; and, 4) the mantle has a MASH composition, we have demonstrated that: 1) a DSZ zone and interplane seismic clusters are highly comparable topologically with dehydration in a hydrous subducting mantle; and , 2) the morphology of a subduction zone depends on the thermal structure of the slab. These observations, at least, support the dehydration-induced earthquake hypothesis, although this logic is a circular argument. In the following sections, we discuss the probability of the assumptions, as well as the possible presence of CO_2, an insight to the thermal structure of a subducting slab, and implications for deep (>400 km) earthquakes.

Role of dehydration for intermediate-depth earthquake

Our first assumption is that any dehydration reaction in a subducting slab induces earthquakes. Two ideas have been suggested to explain how dehydration induces seismicities. One is that the volume change of a reaction causes an earthquake, and another is that dehydration causes stress relaxation by releasing fluid. The former model considers that dehydration itself breaks the rock instead of ambient stress. The dehydration reactions related to intraslab earthquakes have a negative slope at a depth $>$ 80 km (Fig. 10); therefore, the volume change of dehydration is expected to be negative according to Clausius-Clapeyron's equation. Thus, if the volume change causes a break in the rock, the break may be induced by implosion, instead of explosive hydraulic fracturing by increasing the pore pressure on dehydration. Focal mechanism analysis in NE Japan has shown that the upper plane event exhibits down-dip compression, whereas the lower plane event shows

down-dip tension (e.g. Hasegawa *et al.*, 1978; Kosuga *et al.*, 1996), although, in the subduction zone in northern Chile, it is reported that the relationship between the focal mechanism and the two planes is inverted (Comte and Suarez, 1994). According to the analysis by Kosuga *et al.* (1996), most interplane earthquakes in NE Japan show upper plane-type focal mechanisms. This observation suggests that some mechanical factor may contribute to the formation of intraslab earthquakes. The self-implosion model for dehydration inducement does not explain the difference in focal mechanism between upper and lower plane earthquakes.

The latter model, in which dehydration causes stress relaxation and therefore embrittlement of serpentine, was experimentally observed by Raleigh and Paterson (1965) and Meade and Jeanloz (1991), and was adopted for the genesis of DSZ by Seno and Yamanaka (1996) and Peacock (2001). Raleigh and Paterson (1965) suggested two possible mechanisms of dehydration embrittlement of serpentine: 1) reduction of confining pressure by increasing pore pressure of water; and, 2) loss of cohesive strength. Both models consider that fluid formation is essential and are nearly independent from the host material of dehydration.

Meade and Jeanloz (1991) emphasized the significance of the shear displacement of atoms during dehydration, and suggested that a hydrous silicate of a similar structure to serpentine group minerals (e.g. talc, pyrophyllite) may exhibit similar behavior to serpentine. In the present study, antigolite-free dehydration reactions relevant to intraslab earthquakes involve clinochlore or MgMgAl-pumpellyite. Clinochlore is an end-member of chlorite and is a sheet silicate, as is antigorite, but MgMgAl-pumpellyite belongs to a different silicate group (Artioll *et al.*, 1999).

From the discussions above, we can conclude that the formation of a fluid is essential for dehydration embrittlement, thus not only dehydration of antigolite but most dehydration may act as a trigger for seismicities in the slab peridotite, whatever mechanical stress exists. Therefore, our assumption that any dehydration in a subducting slab induces an earthquake is reasonable.

Is subducting mantle really hydrated?

Our second and most critical assumption, i.e., the subducting mantle is hydrated, is the most controversial part of the dehydration-induced earthquake hypothesis. Hydration of the sub-oceanic uppermost mantle has been much discussed since Hess (1962). The petrogenesis of MORB strongly suggests an almost dry mantle at the depth range 30–20 km at a mid-ocean ridge. However, a few possible mechanisms have been proposed to account for the hydration of oceanic lithospheric mantle during its traverse from a mid-ocean ridge to a subduction zone. Seno and Yamanaka (1996) considered hotspot magmatism as a source of water in the oceanic mantle. They envisaged hydration of the oceanic mantle by water released from solidifying magma within the plate. However, it is difficult to explain the extent of dehydration by a hotspot model, because a single hot spot should leave a 1-dimensional trace on the oceanic plate, whereas the extent of hydration in the oceanic lithosphere is expected to be at least 2-dimensional, albeit heterogeneous. Wessel (1997) identified small widespread seamounts in the Pacific plate from Geosat satellite imaging. If these minor seamounts in the Pacific ocean are taken into account, the spatial problem of the hotspot model may be solved. However, the amount of water released from a solidifying magma is less at a great depth, because the solubility of water in the melt generally increases at a higher pressure. Moreover, a magma reservoir is present within the crust at depth and not in the mantle. Even if some magma solidifies in the oceanic mantle, water may be fixed in the rock, probably as amphibole. Thus, we consider that extensive hydration of the oceanic mantle is hardly explained by the hotspot model.

As an alternative source of water, Peacock (2001) proposed deep seawater injection along a major fault in a subducting plate ruptured by a trench-outer rise event. The close association between a double seismic zone and a present-day deep event beneath the trench-outer rise was described by Seno and Yamanaka (1996). Kanamori (1971) suggested that big normal faulting caused by bending of the lithosphere may rupture the oceanic plate for up to a depth of 70 km below the trench; however, the observed maximum depth of the outer-rise event is limited to ca. 50 km (Seno and Yamanaka, 1996). If the fault reaches that depth, and if water can infiltrate through such a fault, the oceanic mantle might be sufficiently hy-

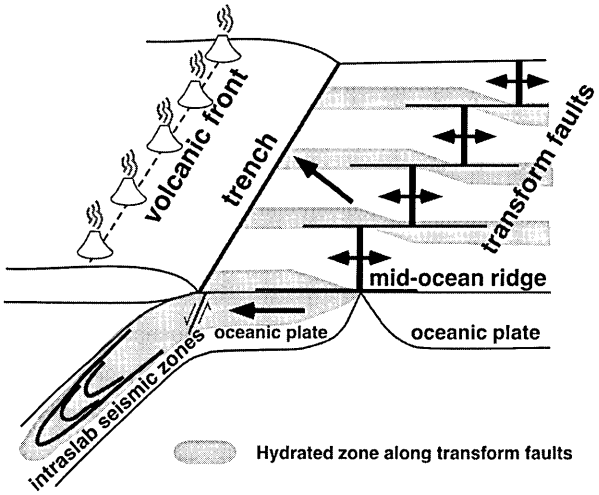

Fig. 15. A depiction of hydration in transform faults and traveling oceanic plate.

drated to the depth of the lower plane of double seismic zone. However, crack sealing by the interaction of wall rock and water may be a possible barrier to the deep penetration of sea water via an outer-rise fault. Neverthless, if the frequency of outer-rise faulting is not rare on a geological time-scale, successively formed new faults would provide the resultant extensive hydration of slab peridotite.

Considering seawater infiltration to oceanic mantle via a fault, transform fault, or oceanic fracture zone may be another way for water to penetrate the slab mantle. The possible penetration of seawater into the oceanic mantle via a transform fault was reported by Francis (1981), and high-temperature alteration of ultramafics in the upper-mantle beneath a fracture zone by Kimball *et al.* (1985). Although the depth-limit of the penetration of the sea water through a transform fault or fracture zone is unknown, it would be higher than via an outer-rise fault, because transform faulting is a continuous event, so crack sealing during infiltration may be prevented.

In Fig. 12, the hypocental distribution of intraslab earthquakes in NE Japan differs from section to section; sections B, C, F, and G exhibit a distinct lower seismic plane, sections A and D lack the lower plane, and separation of the upper and lower planes is not clear in section E. Additionally, the number and the distribution of interplane earthquakes are also different section by section (Fig. 13). If earthquakes are induced by dehydration, such regional heterogeneity of hypocenter distribution in NE Japan suggests a different degree of hydration of the mantle in the various sections. If a transform fault is a source of water, the hydrated part may indicate the wall trace, the strike of which is parallel to the plate movement in NE Japan (Fig. 15). This expected mode of hydration via a transform fault is consistent with the observed heterogeneity of hypocenter distribution in NE Japan, assuming dehydration-induced seismicity.

Although possible mechanisms of the hydration of oceanic mantle have been proposed from different evidence, it is not sufficient to assume that hydrated slab peridotite exists even at a depth of 30 km. Seismic tomography with a calculated Poisson's ratio is the only current method that can provide evidence for deep hydration in the oceanic mantle (Kamiya and Kobayashi, 2000). We have applied this method to the Kanto area, near Tokyo, where the Pacific plate is subducting and a distinct DSZ is observed (Fig. 16). Poisson's ratio is well known to be sensitive to the modal ratio of minerals in a rock, particularly the degree of serpentinization. The values of Poisson's ratio (σ) for various rocks are reported by Christensen (1996). Assuming the hydrous mantle is a mixture of two end-members, dry peridotite ($\sigma=0.25$) and completely hydrated serpentinite ($\sigma=0.35$), the modal amount of serpentine is proportional to Poisson's ratio. Fig. 16 shows seismic tomographic images, the velocities of P and S waves, and Poisson's ratio in a NS cross-section of the Kanto area. The Pacific plate (PAC) is subducting from east to west, and the Philippine Sea plate (PHS) is subducting from south to north vertical to this section (see bottom figure of Fig. 16). The seismic clusters beneath the forearc represent earthquakes in the PHS. Areas of high-Poisson's ratio are observed at: 1) the mantle wedge beneath the volcanic front; 2) above the PHS; 3) within subducting PAC at a depth range from 40–90 km, to ca. 100 km on the lower seismic plane, and 120–140 km between the double seismic planes; and, 4) beneath the PAC. These areas possibly represent heterogeneity in the mantle. 1) may represent partially molten peridotite as a source of arc volcanism. 2) and 3) correspond to partially serpentinized peridotite. One possible interpretation of the area 4) is that it corresponds to the head of an upwelling plume which starts from a minimum depth of 660 km. The

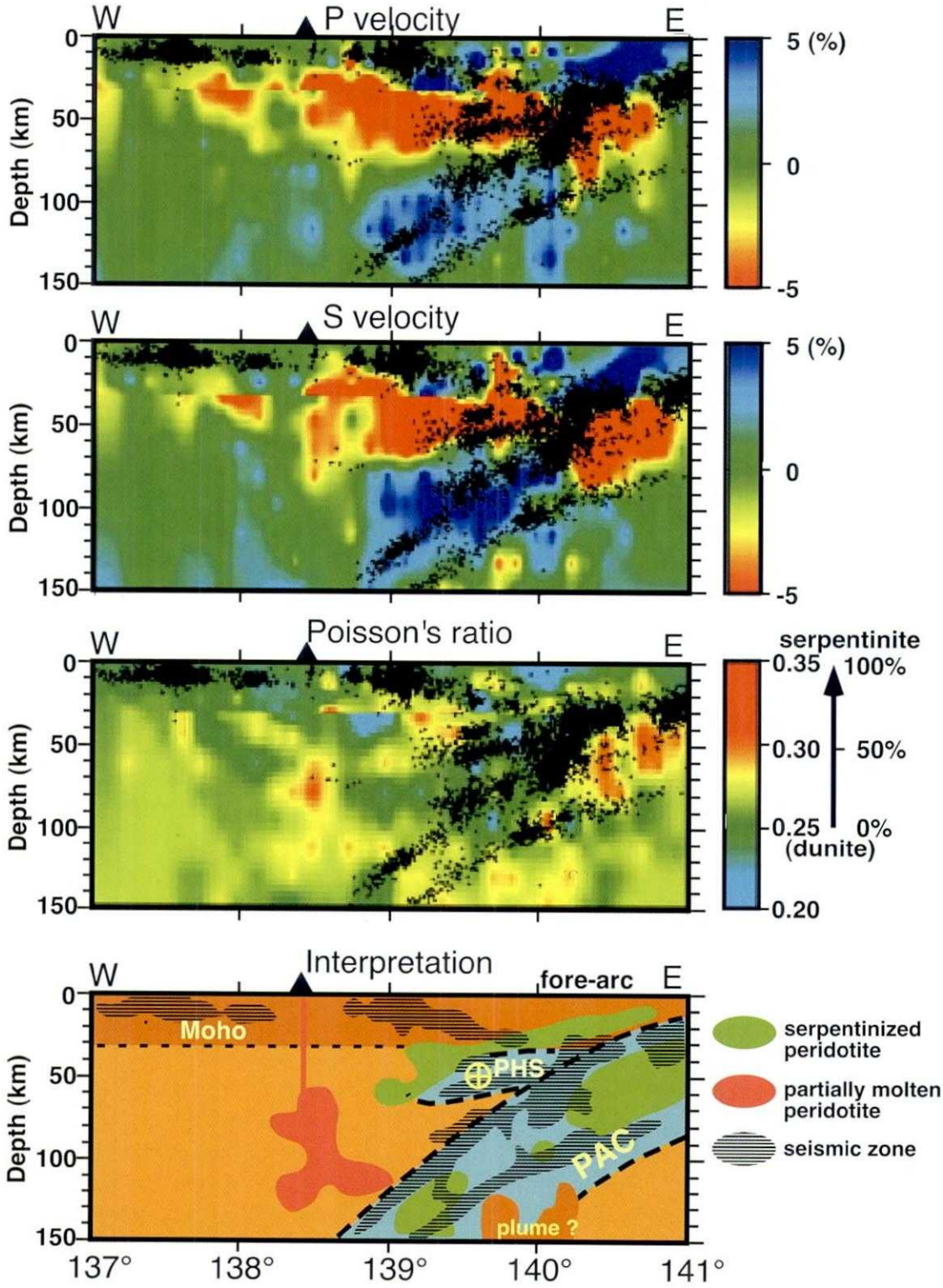

Fig. 16. Seismic tomography of the Kanto area (southern end of NE Japan), showing P-wave velocity, S-wave velocity, Poisson's ratio, and interpretation. PAC: Pacific plate, PHS: Philippine sea plate.

maximum degree of serpentinization is estimated to reach 50% (vol.), assuming a linear correlation of Poisson's ratio to the modal proportion of serpentine in peridotite. We emphasize that the elongated portion of serpentinized slab peridotite continues downwards, following the lower seismic plane (Fig. 16). The seismic tomography of a DSZ indicates the possible existence of serpentinite in slab peridotite, and this supports the assumption of a hydrated mantle.

Uncertainty of hypocenter location, kinetic effect, and continuous reaction

The third and fourth of our assumptions, equilibrium dehydration and MASH mantle, are related to the link between dehydration and hypocenter distribution. Hypocenter distribution in NE Japan seems to have a good correlation with dehydration reaction; however, as shown in Figs. 9 b and 9 c, peaks of interplane earthquakes have a relatively broad range and there are minor seismicities where no dehydration is expected. These discrepancies from the prediction are considered to be due to a combination of uncertainties: 1) hypocenter location, 2) kinetic effect on the dehydration reaction and, 3) effect of continuous reaction. The precision of the hypocenter location is considered to be sufficient for the required accuracy of the present study. Earthquake data provided by the Japan University Network Earthquake Catalog, which are deeper than 50 km, contain uncertainty in the location of the hypocenter with a maximum $\pm$10 km. The difference of 10 km in depth corresponds to a difference in pressure of ca. 0.3 GPa in the P-T diagram. This uncertainty may have some effect on the morphology of the DSZ; therefore, the morphological discussion of the hypocenter distribution must be larger in scale than this uncertainty.

The assumption of equilibrium dehydration is considered to be reasonable, because numerous studies on metamorphic rocks have indicated that dehydration in the prograde stage may take place at P-T condition just above the equilibrium curve (e.g. Spear, 1993; Miyashiro, 1994). Therefore, the uncertainty, based on the kinetic effect, is considered to be small if the slab is hydrated; and, the predicted reaction topology in the model slab may represent actual dehydrations in a natural subduction zone.

The compositional difference between natural rock and the assumed MASH model system may be the most dominant cause of a broader hypocenter distribution compared to the prediction from a MASH model system. Natural serpentinite contains some Fe and Ca, in addition to the model MASH system. Incorporation of these components into the phase equilibria turns the individual reactions into a continuous reaction that includes solid solution (e.g. Mg-Fe substitution in antigorite, talc, enstatite; and Ca-Mg-Fe substitution in garnet); a continuous reaction occurs in a specific range of P-T conditions, but not on a univariant curve. Some part of the broader distribution of interplane earthquakes than the prediction is considered to represent the range of continuous reactions, although the range is not estimated quantitatively due to a lack of both experimental and thermodynamic data for Fe end-members of antigorite, phase A, etc.

Other volatile component: CO_2

In previous sections, we considered the volatile component in the subducting mantle to be only H_2O. However, the presence of CO_2 in shallow serpentinization in a fracture zone of the mid-Atlantic ridge was reported by Charlou *et al.* (1998). This observation suggests that CO_2 is also a possible volatile component, if the hydration of deep upper mantle is induced by the penetration of sea water. Kirby (1995) also suggested CO_2 in the subducting slab mantle. He proposed that a possible cause of lower plane earthquakes was reactivation of a fault by decarbonation of carbonate along it. As discussed in the previous section, the formation of a fluid plays an important role in the embrittlement of a rock; therefore devolatilization including CO_2 can be a candidate to trigger an intraslab earthquake. Therefore, we calculated the position of possible CO_2-bearing devolatilization in the subducting mantle in a P-T space and compared it to the distribution of interplane earthquakes. The P-T diagram in Fig. 17 shows the correlation between the depths of interplane earthquakes in NE Japan and possible dehydration and additional CO_2-bearing devolatilization. The primary carbonate coexisting with antigorite was assumed to be $CaCO_3$. The devolatilization reactions including CO_2 occur in a depth range of ca. 80–100 km, which corresponds to the shallower cluster of interplane earthquakes. This result provides a better link between interplane earthquakes and fluid formation than the MASH model, because a broad peak at 85–135 km is interpreted to be the combination of a carbonate-bearing

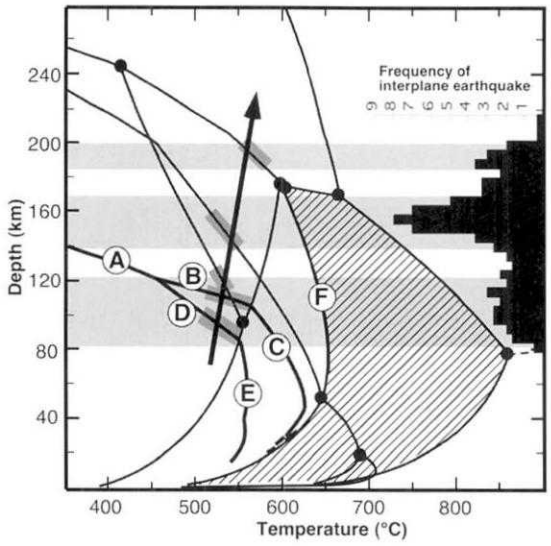

Fig. 17. P-T diagram in the system MASH + $CaCO_3$ with superimposed depth-frequency relation of interplane earthquakes in the cross-section in Fig. 8. Light shaded areas represent possible pressure conditions of the interplane earthquakes. Dark shaded areas are P-T conditions where reaction curves intersect the pressure of interplane earthquakes. Arrows are possible P-T paths for coldest thermal center of the slab.
Reactions: A: Atg + Arag = Br + Mag + Di + Fld; B: Atg + Do = Br + Mag + Di + Fld; C: Atg + Do = Mag + Fo + Di + Fld; D: Atg + Arag = Br + Do + Di + Fld; E: Atg + Tc + Do = Mg + Tr + Fld, F: Atg + Mag = En + Fo + Fld.

reaction and dehydration of antigorite + brucite. By including carbonates in the calculation, we achieved a better link between the prediction and observations of the intraslab earthquakes. This result supports the idea that CO_2 should be included as a volatile component of hydrated mantle.

Thermal structure of the subducting slab

We have compared dehydrations with intermediate-depth earthquakes using multiple reactions and multiple seismic zones, and estimated a P-T path of the coldest thermal center. Fig. 18a shows a superimposed possible location of dehydration reactions on a cross-section of NE Japan, assuming the P-T path (I) for the coldest thermal center in Fig. 10. The estimated isotherm from Fig. 18a is drawn in Fig. 18b. Our result is remarkably different from the numerically simulated thermal structure (Fig. 18c). Our estimate indicates a distinctly higher temperature on the inside of the slab, even taking into account the considerable uncertainty in the phase dia-

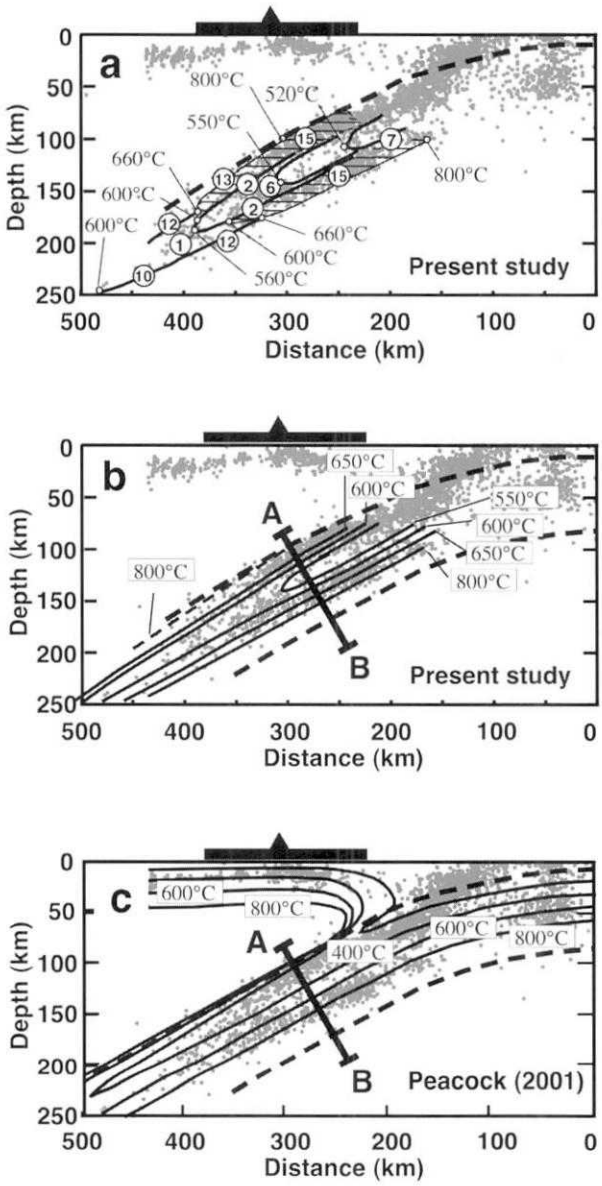

Fig. 18. a) Hypocenter distribution in NE Japan with superimposed dehydration reactions; b) estimated thermal structure of northeast Japan on the basis of our dehydration-induced earthquake model; and, c) numerically simulated thermal structure of NE Japan by Peacock (2001). Temperature distribution along A-B profile is shown in Fig. 19.

gram and the observations. The temperature difference reaches ca. 250°C. If this is correct, the discrepancy must be derived from the model and the arbitrary choice of parameters used in the numerical simulations.

Figure 19 shows the temperature profile across the slab according to our estimate compared to the numerical simulation of Peacock (2001). According to Peacock (2001) the temperature difference is maxi-

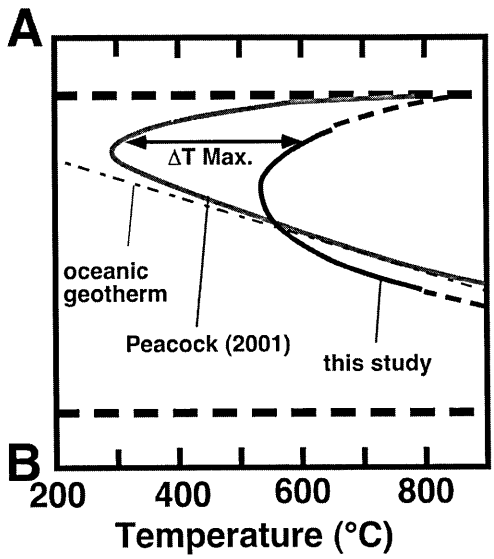

Fig. 19. Comparison of thermal profiles across the slab A-B section in Fig. 18. black curve: estimated temperature from this study. gray curve: temperature obtained by numerical simulation of Peacock (2001), thin dashed line: oceanic geotherm of the Pacific plate in front of the trench, thick dashed line: slab boundary.

mum on the inside of the slab at ca. 20 km from the upper boundary, and it is minimum near the slab boundary. Our estimate requires more heating on the inside of the slab than the calculation of Peacock (2001). Parameters, which could contribute significant uncertainty to the degree of heating to the slab, are thermal conductivity and viscous heating. If the thermal conductivity of the slab upper boundary is higher than that used in the simulation, the inside of the slab may become warmer due to conductive heat from the mantle wedge. Shear stress causing frictional heating would also produce additional heat. According to the thermal model of the subducting slab by Peacock (1996), shear stress is one of the most dominant parameters used to define the thermal structure of the subducting slab by thrust heating at shallower depth (ca. <70 km). Because shear stress is not an observable parameter, it may contribute to uncertainty in the calculation. If heating inside the slab is due to high frictional heat, the temperature difference between the observations and the simulation should also be large at the upper boundary of the slab. Thus the temperature of the slab upper boundary is also important to constrain the thermal parameter of the slab. However, our estimate is based on the link between dehydration and the seismic zone in peridotite; therefore, the temperature in MORB at the upper boundary of the slab is not relevant. If the isotherm estimated in peridotite is simply extended to the MORB crust (dashed line in Fig. 18 and Fig. 19), the temperature difference becomes smaller near the upper boundary of the slab.

A possible interpretation of the relatively colder slab surface is that a low-T hydrous fluid derived from dehydration underneath the slab cooled the upper portion of the slab. Fluids released from the colder interior of the slab may move upwards to refrigerate the upper portion of the slab. Although we do not discuss the thermal modeling of the slab quantitatively, our estimate of the thermal structure of the slab on the basis of the dehydration-induced earthquake hypothesis suggests that a re-evaluation of parameters, thermal conductivity, and shear stress, and of the modeling that includes heat transport by fluid from inside the slab, is necessary for more precise thermal modeling of a subduction zone.

Deep earthquakes

We have discussed the dehydration-induced earthquake model for intermediate depths in the previous sections. It is well known that most subduction zones with intermediate depth earthquakes also have deep earthquakes in the range from ca. 400 km to 700 km, except those with young plates (Fig. 20). In previous studies, it has been suggested that metastable phase transformation of olivine in dry- and cold-subducting peridotite induces earthquakes at a depth greater than 410 km (e.g. Green and Burney, 1989). This model is based on the assumption that a very cold subducting slab prevents equilibrium phase transformation; and, the temperature of 600℃ is a critical temperature for initiating metastable olivine transformation in the equilibrium stability field of high-P phase. However, in the present study, we estimated that the temperature of the slab is higher than 600℃ at a depth of 400 km. Therefore, our dehydration-induced earthquake model is inconsistent with the metastable transformation model for deep earthquakes; consequently, it is necessary to provide another model for the origin of deep earthquakes. In this section, we show that the dehydration-induced earthquake model is also applicable to deep earthquakes.

Figure 21 is a P-T diagram showing possible dehydration reactions and superimposed depth-

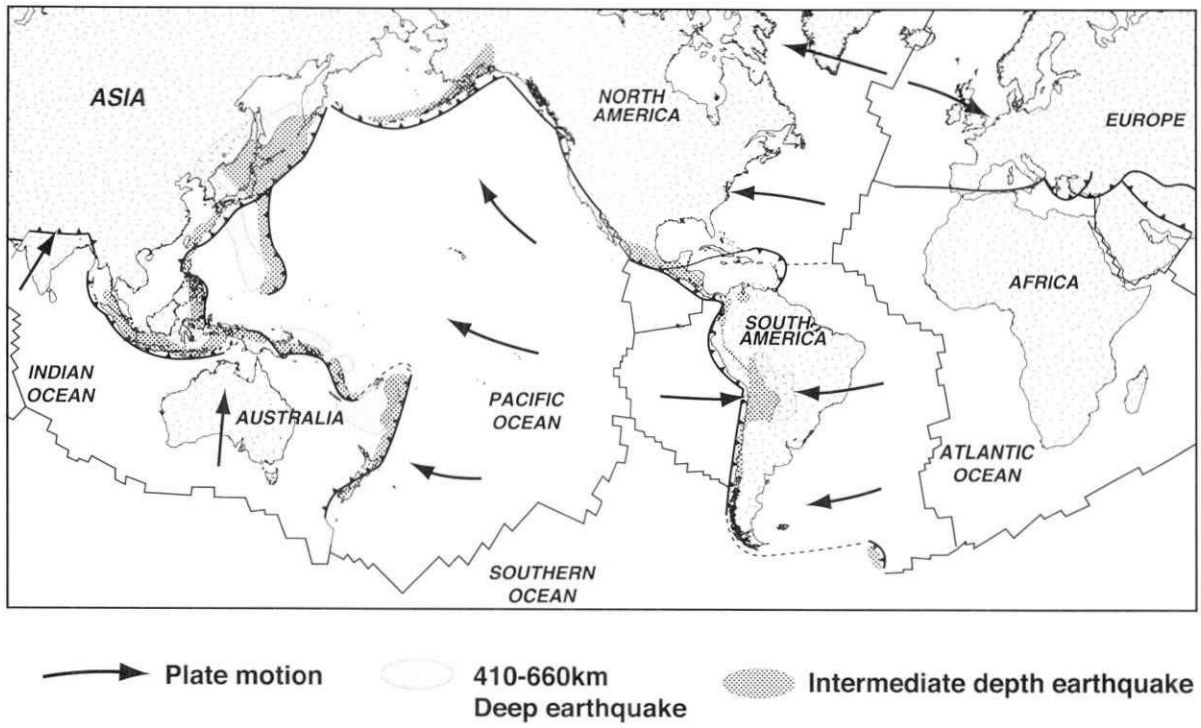

Fig. 20. World-distribution of deep and intermediate depth earthquakes.

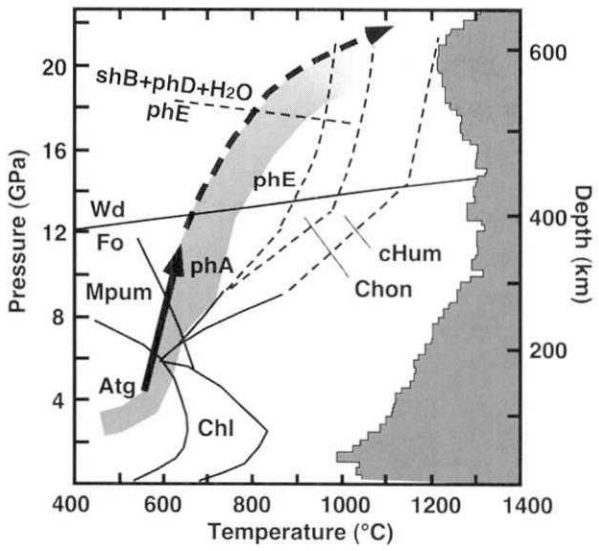

Fig. 21. P-T diagram showing depth-frequency relations of whole-subduction zone earthquakes (after Kirby, 1995) and dehydration reactions in hydrated mantle. Solid lines: dehydration curves estimated from the present study. Dashed lines: approximate location of dehydration reactions estimated from the experiments of Irifune *et al.* (1998) and Stalder and Ulmer (2001). Shaded areas are approximate P-T range of the hydrous portion of subducting lithosphere. Abbreviations: phD: phase D, phE: phase E, shB: super hydrous phase B.

frequency relations of the whole world's subduction zone earthquakes. A high frequency of earthquakes in the depth range of ca. 0–300 km corresponds to shallow and intermediate-depth earthquakes. The depth range of 300–450 km is characterized by the less seismicity. Although it is known that dense hydrous magnesian silicates (DHMS) are still stable in this depth range (Irifune *et al.*, 1998), the steep P-T path cannot cross a dehydration reaction and dehydration does not occur in the subducting slab after decomposition of antigorite or MgMgAl-pumpellyite. We suggest the lack of dehydration represents fewer earthquakes in this depth range.

The second frequency peak of the earthquakes is at a depth of about 600 km, which is close to the 660 km thermal boundary, where ringwoodite transforms to perovskite+wüstite. The phase transition at 660 km has a negative Clapeyron slope, thus the subducted cold peridotite may stagnate at this boundary. Moreover, the viscosity difference between the upper and lower mantle reaches two orders of magnitude; this observation also suggests a stagnant slab at 660 km. A stagnant slab at 660 km was also demonstrated by P-wave tomography underneath NE Japan by Fukao (1992). A steep tem-

perature gradient between the lower mantle and the overlying subducted slab is expected at the 660 km boundary, thus the cold subducted slab must be affected by conductive thermal heating from the lower mantle at a nearly isobaric condition (P-T path indicated by dashed arrow in Fig. 21). In this depth range, dehydration of phase E is at ca. 17 GPa by high-pressure experiments with peridotite+H_2O (Kanzaki, 1991; Ohtani *et al.*, 1995) and serpentine bulk composition (Irifune *et al.*, 1998) (Fig. 21). Chondrodite and clinohumite are also possible candidates for the source of dehydration (Stalder and Ulmer, 2001), although the stabilities of these minerals are not confirmed at this depth. Isobaric heating in a stagnant slab may easily induce dehydration of these minerals at a depth of about 600 km.

From the above discussion, deep earthquakes seem to have corresponding dehydrations, thus the dehydration model adequately explains deep earthquakes, as well as intermediate-depth earthquakes, although we need a more precise determination of the position of dehydration with high-pressure experiments, and a better evaluation of the thermal structure of the subducted slab in the mantle transition zone.

Conclusions

We applied dehydration phase equilibria of hydrated mantle in the MASH system to the morphology of the intraslab seismic zone. The following five results came from the present study.

1) The whole morphology of a double seismic zone, including the depth distribution of interplane earthquakes, is closely correlated with the P-T condition of dehydration reactions in the subducting slab peridotite. The structure of the intraslab seismic zone at intermediate depths is probably controlled by dehydration reactions including serpentine, brucite, talc, clinochlore, and MgMgAl-pumpellyite.

2) The assumption of hydrated mantle down to depth of 30–40 km in the oceanic lithosphere is confirmed from the distribution of Poisson's ratio in a subduction zone and seismic tomography.

3) Decarbonation reactions are also considered to be one of the sources of intraslab earthquakes. The earthquakes at about 100 km in depth probably correspond to the decarbonation in the subducting peridotite.

4) The thermal strucure of the subducting slab in NE Japan is estimated from the link between dehydration and the seismic zones. Our estimated temperature is significantly higher than that derived from a numerical simulation. The thermal parameter of a slab, e.g., shear stress and conductivity, should be re-evaluated.

5) Our dehydration-induced earthquake model is also applicable to deep earthquakes (>400 km). Detailed determination of the P-T positions of the dehydration of phase E, clinohumite, and chondrodite, and a new insight into the thermal structure of the subducted mantle in the transition zone require further discussion of the dehydration-induced deep earthquake model in the future.

Acknowledgements

The authors thank B. Windley for improving the manuscript. We are grateful to J. Kasahara, S. Kirby, H. Green, and H. Iwamori for fruitful discussions, and thank J.G. Liou and Y. Ogasawara for their encouragement through this study. Critical reviews by T. Seno and M. Toriumi further improved the manuscript.

References

Artioli, G., P. Fumagalli and S. Poli, 1999, The crystal structure of Mg_8 (Mg_2Al_2) Al_8Si_{12} (O, OH)$_{56}$ pumpellyite and its relevance in ultramafic systems at high pressure, *American Mineralogist*, **84**, 1906–1914.

Barazangi, M and B. Isacks, 1979, A comparison of the spatial distribution of mantle earthquakes determined from data produced by local and by teleseismic networks for the Japan and Aleutian arcs, *Bulletin of Seismological Society of America*, **69**, 1763–1770.

Bose, K. and A. Navrotsky, 1998, Thermochemistry and phase equilibria of hydrous phases in the system MgO-SiO_2-H_2O: Implications for volatile transport to the mantle, *Journal of Geophysical Research*, **103**, 9713–9719.

Christensen, N., 1996, Poissons's ratio and crustal seismology, *Journal of Geophysical Research*, **101**, 3139–3156.

Comte, D. and G. Suarez, 1994, An inverted double seismic zone in Chile: Evidence of phase transformation in the subducted slab, *Science*, **263**, 212–215.

Engdahl, E.R. and C.H. Scholz, 1977, A double Benioff zone beneath the central Areutians: An unbending of lithospere, *Geophysical Research Letters*, **4**, 473–476.

Faust, J. and E. Knittle, 1994, Static compression of chondrodite: Implications for water in the upper mantle, *Geophysical Research Letters*, **21**, 1935–1938.

Fockenberg, T., 1998, an experimental study of the pressure-temperature stability of MgMgAl-pumpellyite in the system MgO-Al_2O_3-SiO_2-H_2O, *American Mineralogist*, **83**,

220-227.

Francis, T.J.G., 1981, Serpentinization faults and their role in the tectonics of slow spreading ridges, *Journal of Geophysical Research,* **86**, 11616-11622.

Fukao, Y., 1992, Seismic tomogram of the Earth's mantle: geodynamic implications, *Science,* **258**, 625-630.

Gorbatov, A., G. Suarez, V. Kostoglodov and E. Gordeev, 1994, A double-planed seismic zone in Kamchatka from local and teleseismic data, *Geophysical Research Letters,* **21**, 1675-1678.

Gorbatov, A. and V. Kostoglodov, 1997, Maximum depth of seismicity and thermal parameter of the subducting slab: general emprical relation and its application, *Tectonophysics,* **277**, 165-187.

Green II, H.W. and P.C. Burney, 1989, A new self organizing mechanism for deep-focus earthquakes, *Nature,* **341**, 733-737.

Hasegawa, A., N. Umino and A. Takagi, 1978, Double-planed structure of the deep seismic zone in the northeastern Japan arc, *Tectonophysics,* **47**, 43-58.

Hasegawa, A., S. Horiuchi and N., Umino, 1994, Seismic structure of the northeastern Japan convergent plate margin: A synthesis, *Journal of Geophysical Research,* **99**, 22295-22311.

Hess, H.H., 1962, History of ocean basins, in petrological studies: A volume in Honor of A.F. Buddington, eds. A. E. Angel *et al.,* GSA, 599-620.

Holland, T.J.B. and R. Powell, 1998, An internally consistent thermodynamic dataset for phases of petrological interest, *Journal of Metamorphic Geology,* **16**, 309-343.

Hori, S., 1997, Earthquake mechanism within the Philippine Sea plate subducting beneath the Kanto district, *central Japan, Jisin,* **50**, 203-213, (in Japanese).

Iidaka, T. and Y., Furukawa, 1994, Double seismic zone for deep earthquakes in the Izo-Bonin subduction zone, *Science,* **263**, 1116-1118.

Irifune, T., N. Kubo, M. Isshiki and Y. Yamasaki, 1998, Phase transformations in serpentine and transportation of water into the lower mantle, *Geophysical Research Letters,* **25**, 203-206.

Iwamori, H., 1998, Transportation of H_2O and melting in subduction zones, *Earth and Planetary Science Letters,* **160**, 65-80.

Kamiya, S. and Y. Kobayashi, 2000, Seismological evidence for the existence of serpentinized wedge mantle, *Geophysical Research Letters,* **27**, 819-822.

Kanamori, H., 1971, Seismological evidence for a lithospheric normal faulting -The Sanriku earthquake of 1933, *Physics of the Earth and Planetary Interiors,* **4**, 289-300.

Kanzaki, M., 1991, Stability of hydrous magnesium silicate in the transition zone, *Physics of Earth and Planetary interior,* **66**, 307-312.

Kao, H. and W.P. Chen, 1994, Double seismic zone in Kuril-Kamchatka: The role of two overlapping single seismic zones, *Journal of Geophysical Research,* **99**, 6913-6930.

Kao, H. and L.G. Liu, 1995, A hypothesis for the seismogenesis a double seismic zone, *Geophysical Journal International,* **123**, 71-84.

Kawakatsu, H., 1985, Double seismic zone in Tonga, *Nature,* **316**, 53-55.

Kawakatsu, H., 1995, Downdip tensional earthquakes beneath the Tonga arc: A double seismic zone ?, *Journal of Geophysical Research,* **91**, 6432-6440.

Kimball, K.L., F.S. Spear and H.J.B. Dick, 1985, High temperature alteration of abyssal ultramafics from the Islas Orcadas fracture zone, South Atlantic, *Contributions to Mineralogy and Petrology,* **91**, 307-320.

Kirby, S., 1995, Intraslab earthquakes and phase changes in subducting lithosphere, *Reviews in Geophysics*, supplement, 287-297.

Kirby, S., W.B. Durham and L.A. Stern, 1991, Mantle phase changes and deep-earthquake faulting in subducting lithosphere, *Science,* **252**, 216-225.

Kosuga, M., S. Suzuki, Y. Motoya, T. Sato, A. Hasegawa and T. Matsuzawa, 1996, Spatial distribution of intermediate-depth earthquakes with horizontal or vertical nodal planes beneath northeastern Japan, *Physics of the Earth & Planetary Interiors,* **93**, 63-89.

McGuire, J.J. and D.A. Wiens, 1995, A double seismic zone in New Britain and the morphology of the Solomon plate at intermediate depth, *Geophysical Research Letters,* **22**, 1965-1968.

Meade, C. and R. Jeanloz, 1991, Deep-focus earthquakes and recycling of water into Earth's mantle, *Science,* **252**, 68-72.

Miyashiro, A., 1994, Metamorphic Petrology, UCL Press, London.

Nishiyama, T., 1992, Mantle hydrology in a subduction zone : A key to episodic geologic events, double Wadati-Benioff zones and magma genesis, in Mathmatical Seismology VII, *Report of The Institute of Statistical Mathematics, Tokyo,* **34**, 31-67.

O'Hanley, D.S., 1996, Serpentinites: records of tectonic and petrological history, Oxford monographs of geology and geophysics, 34, Oxford University Press, Oxford.

Ohtani, E., T. Shibata, T. Kubo and T. Kato, 1995, Stability of hydrous phases in the transition zone and the uppermost part of the lower mantle, *Geophysical Research Letters,* **22**, 2553-2556.

Omori, S. and Y. Ogasawara, 1998, "UniEQ": A computer program package for constructing petrogenetic grids, *EOS,* **79**, F999.

Omori, S., T. Komabayashi and S. Maruyama, 2000, Intraslab seismic zone morphology and devolatilization phase equilibria of the subducting slab, *EOS,* **81**, F1372.

Ozel, N. and T. Moriya, 1999, Different stress directions in the aftershock focal mechanisms of the Kushiro-Oki earthquake of Jan. 15, 1993, SE Hokkaido, Japan, and horizontal rupture in the double seismic zone, *Tectonophysics,* **313**, 307-327.

Paterson, M.S., 1978, Experimental rock deformation -the brittle field, Springer-Verlag, Berlin, 254 pp.

Pawley, A., 2000, Stability of clinohumite in the system MgO-SiO_2-H_2O, *Contributions to Mineralogy and Petrology,* **138**, 284-291.

Peacock, S. , 1996, Thermal and petrologic structure of subduction zones, in Bebout *et al.* eds., Subduction Top to Bottom, *American Geophysical Union Geophysical Monograph,* **96**, 119-133.

Peacock, S., 2001, Are the lower planes of double seismic zones caused by serpentine dehydration in subducting

oceanic mantle ?, *Geology*, **29**, 299-302.

Raleigh, C.B. and M.S. Paterson, 1965, Experimental deformation of serpentinite and its tectonic implications, *Journal of Geophysical Research*, **70**, 3965-3985.

Ratchkovsky, N.A., J. Pujol and N.N. Biswas, 1997, Stress pattern in the double seismic zone beneath Cook Inlet, south-central Alaska, *Tectonophysics*, **281**, 163-171.

Seno, T. and Y. Yamanaka, 1996, Double seismic zones, compressional deep trench-outer rise events, and superplumes, in Bebout *et al.* eds., Subduction Top to Bottom, *American Geophysical Union Geophysical Monograph*, **96**, 347-355.

Seno, T., D. Zhao, Y. Kobayashi and M. Nakamura, 2001, Dehydration of serpentinized slab mantle: Seismic evidence from southwest Japan, *Earth, Planets and Space*, **53**, 861-871.

Shinmei, T., N. Tomioka, K. Fujino, K. Kuroda and T. Irifune, 1999, In situ X-ray diffraction study of enstatite up to 12 GPa and 1473 K and equations of state, *American Mineralogist*, **84**, 1588-1594.

Spear, F., 1993, Metamorphic phase equilibria and pressure-temperature-time paths, Mineralogical Society of America, Monograph, Washington.

Stalder, R. and P. Ulmer, 2001, Phase relations of a serpentine composition between 5 and 14 GPa: significance of clinohumite and phase E as water carriers into the transition zone, *Contributions to Mineralogy and Petrology*, **140**, 670-679.

Ulmer, P. and V. Trommsdorff, 1995, Serpentine stability to mantle depths and subduction-related magmatism: *Science*, **268**, 858-861.

Ulmer, P. and V. Trommsdorff, 1999, Phase relations of hydrous mantle subducting to 300 km, in *Mineral Spectroscopy*, The Geochemical Society, Special Publication, 6, pp. 1-23.

Umino, N. and A. Hasegawa, 1975. On the two-layered structure of deep seismic plane in northeastern Japan arc (in Japanese with English abstract), *Journal of Seismological Society of Japan*, **27**, 125-139.

Wessel, P., 1997, Sizes and ages of seamounts using remote sensing: Implications for intraplate volcanism, *Science*, **277**, 802-805.

Wunder, B., 1998, Equilibrium experiments in the system MgO-SiO_2-H_2O (MSH): stability fields of clinohumite-OH [$Mg_9Si_4O_{16}(OH)_2$], chondrodite-OH [$Mg_5Si_2O_8(OH)_2$] and phaseA [$Mg_7Si_2O_8(OH)_6$], *Contributions to Mineralogy and Petrology*, **132**, 111-120.

Wunder, B. and W. Schreyer, 1997, Antigorite: High-pressure stability in the system MgO-SiO_2-H_2O (MSH), *Lithos*, **41**, 213-227.

Zhao, D., T. Matsuzawa and A. Hasegawa, 1997, Morphology of the subducting slab boundary in the northeastern Japan arc, *Physics of the Earth and Planetary Interiors*, **102**, 89-104.

(Received August 27, 2001)
(Accepted December 14, 2001)